PLB-985 neutrophil-like cells as a model to study *Aspergillus fumigatus* pathogenesis

Muhammad Rafiq[a,b,#], Flora Rivieccio[a,b,#], Ann-Kathrin Zimmermann[a,b,#], Corissa Visser[a,b], Alexander Bruch[c], Thomas Krüger[a], Katherine González Rojas[a,b], Olaf Kniemeyer[a,b], Matthew G. Blango[c], Axel A. Brakhage[a,b]*

[a] Department of Molecular and Applied Microbiology, Leibniz Institute for Natural Product Research and Infection Biology - Hans Knöll Institute (Leibniz-HKI), Jena, Germany.

[b] Department of Microbiology and Molecular Biology, Institute of Microbiology, Friedrich Schiller University, Jena, Germany.

[c] Junior Research Group RNA Biology of Fungal Infections, Leibniz Institute for Natural Product Research and Infection Biology - Hans Knöll Institute (Leibniz-HKI), Jena, Germany.

Running Title: Neutrophil-like model of *A. fumigatus* infection

Key Words: *Aspergillus fumigatus*, PLB-985, phagocytosis, fungal pathogens, extracellular vesicles, HL-60

*Correspondence: E-mail axel.brakhage@leibniz-hki.de

Tel. +49 (0)3641-532 1001.

# These authors contributed equally to the manuscript and were listed alphabetically

ABSTRACT

Fungal infections remain a major global concern. Emerging fungal pathogens and increasing rates of resistance mean that additional research efforts and resources must be allocated to advancing our understanding of fungal pathogenesis and developing new therapeutic interventions. Neutrophilic granulocytes are a major cell type involved in protection against the important fungal pathogen *Aspergillus fumigatus*, where they employ numerous defense mechanisms, including production of antimicrobial extracellular vesicles. A major draw-back to work with neutrophils is the lack of a suitable cell line system for the study of fungal pathogenesis. To address this problem, we assessed the feasibility of using differentiated PLB-985 neutrophil-like cells as an *in vitro* model to study *A. fumigatus* infection. We find that dimethylformamide-differentiated PLB-985 cells provide a useful recapitulation of many aspects of *A. fumigatus* interactions with primary human polymorphonuclear leukocytes. We show that differentiated PLB-985 cells phagocytose fungal conidia and acidify conidia-containing phagolysosomes similar to primary neutrophils, release neutrophil extracellular traps, and also produce antifungal extracellular vesicles in response to infection. In addition, we provide an improved method for the isolation of extracellular vesicles produced during infection by employing a size-exclusion chromatography-based approach. Advanced LC-MS/MS proteomics revealed an enrichment of extracellular vesicle marker proteins and a decrease of cytoplasmic proteins in extracellular vesicles isolated using this improved method. Ultimately, we find that differentiated PLB-985 cells can serve as a genetically tractable model to study many aspects of *A. fumigatus* pathogenesis.

IMPORTANCE

Polymorphonuclear leukocytes are an important defense against human fungal pathogens, yet our model systems to study this group of cells remains very limited in scope. In this study, we established that differentiated PLB-985 cells can serve as a model to recapitulate several important aspects of human polymorphonuclear leukocyte interactions with the important human fungal pathogen *Aspergillus fumigatus*. The proposed addition of a cultured neutrophil-like cell line to the experimental toolbox to study fungal pathogenesis will allow for a more mechanistic description of neutrophil antifungal biology. In addition, the easier handling of the cell line compared to primary human neutrophils allowed us to use PLB-985 cells to provide an improved method for isolation of neutrophil-derived extracellular vesicles using size-exclusion chromatography. Together, these results provide significant tools and a baseline knowledge for the future study of neutrophil-derived extracellular vesicles in the laboratory.

55 **INTRODUCTION**

56 Fungal infections remain a tremendous source of global morbidity and mortality. More than 1 billion individuals
57 are affected by fungal infections per year, with invasive infections killing numbers comparable to other leading
58 bacterial pathogens (>1.5 million per year; gaffi.org; (1)). Deadly invasive infections are caused by a relatively small
59 number of fungi, with most of these attributed to members of the genera *Candida*, *Pneumocystis*, *Cryptococcus*,
60 and *Aspergillus* (2). *Aspergillus fumigatus* is the major cause of aspergillosis and is particularly dangerous to
61 immunocompromised individuals suffering from neutropenia (3). There is also emerging evidence to suggest that
62 invasive aspergillosis may contribute to COVID-19-related deaths (4, 5), but challenges in safely obtaining
63 bronchoalveolar lavage samples from these patients have often made confirmatory diagnosis difficult. Despite the
64 obvious importance of *A. fumigatus* in the clinic, our understanding of this important pathogen remains lacking in
65 many aspects, in part due to a lack of tractable experimental systems in the laboratory.

66 Mammals are continuously challenged by fungal pathogens. In fact, asexual spores of *A. fumigatus*,
67 termed conidia, are thought to be inhaled by humans on a scale of hundreds per day (6). For most fungi, the body
68 temperature of mammals is too high to allow for growth, but for organisms like *A. fumigatus* that thrive in compost
69 piles at high temperatures, the human host provides fertile ground in the absence of a functional immune system
70 (7). However, humans do have multiple additional defenses, including a mucociliary escalator to remove particles
71 from the lungs, a robust epithelium, resident alveolar macrophages that eliminate the majority of the remaining
72 fungal conidia, and infiltrating polymorphonuclear leukocytes (PMNs) that aid in clearance of conidia and
73 destruction of fungal hyphae, among others (3, 8). Neutrophils play an essential role in antifungal defense, due to
74 their importance in killing fungal hyphae. This is well-illustrated by the high susceptibility of neutropenic patients
75 to *A. fumigatus* infections in the clinics (reviewed in (3, 9)).

76 Studies in primary human neutrophils have revealed the capacity of these cells to phagocytose conidia
77 and release granules, neutrophil extracellular traps (NETs), and extracellular vesicles in response to invading
78 pathogens (10-12). Phagocytosis occurs in conjunction with recognition of pathogen-associated molecular
79 patterns by host pathogen recognition receptors. Studies in zebrafish and mice have shown that these internalized
80 conidia can even be passed from neutrophils to macrophages for destruction of the fungus (13), implying complex
81 intracellular trafficking. In neutrophils and macrophages however, internalized wild-type *A. fumigatus* conidia are
82 capable of stalling phagolysosomal acidification to facilitate outgrowth.

83 In addition to phagocytosis, NETs are an important mechanism of defense against *A. fumigatus* that are
84 produced in response to fungal recognition in a CD11b-dependent manner (11, 14). NET production is most
85 abundant against hyphae, but NETs are also sometimes produced in response to resting and swollen conidia (15).
86 In vivo, NETs were shown to be present in mouse lungs during infection but were generally dispensable for fungal

87 clearance (15, 16), suggesting that alternative measures are required to eliminate fungal hyphae that escaped
88 phagocytosis as conidia.

89 Neutrophilic granules and extracellular vesicles are two heterogeneous subcellular populations that also
90 contribute widely to the antimicrobial response. Proteins like lactoferrin associated with granules are known to
91 inhibit *A. fumigatus* conidial germination due to iron sequestration (17) and the abundant granule protein
92 myeloperoxidase inhibits fungal hyphal growth (18). Extracellular vesicles were also shown to provide an
93 antifungal mechanism against *A. fumigatus* hyphae and conidia (10). Antifungal extracellular vesicles produced by
94 neutrophils in response to infection are capable of associating with the fungal cell wall and are in some cases
95 internalized to deliver an unknown antifungal cargo. Intriguingly, the antifungal effect of these extracellular
96 vesicles appeared to be tailored to the infecting pathogen, as spontaneously released vesicles and vesicles
97 released in response to infection with a knockout strain deficient in production of the conidial pigment
98 dihydroxynaphthalene (DHN)-melanin were not antifungal against wild-type fungus (10).

99 The dissection of the molecular mechanisms behind these differences in antifungal potential are difficult
100 to discern in the absence of a tractable model system for the genetic manipulation of neutrophils. Despite the
101 importance of neutrophils in antifungal defense, the majority of studies are still performed in primary human
102 PMNs isolated from venous blood, a resource that can only be used for small-scale studies and is unfortunately
103 highly variable between blood donors. A laborious isolation procedure and limited half-life of about 19 hours *ex*
104 *vivo* (19) also make more mechanistic studies difficult. For all these reasons, establishment of a cell culture line to
105 study *A. fumigatus* pathogenesis in neutrophils or neutrophil-like cells would be highly advantageous. In recent
106 years some options have emerged to investigate specific aspects of neutrophil biology in culture (20). In particular,
107 the myeloid cell line PLB-985, a derivative of HL-60 granulocytic cells, has recently emerged as a tractable model
108 to study NET formation in response to bacterial infection after differentiation into neutrophil-like cells (21, 22). Of
109 note, the related HL-60 cell line has also been used previously to deliver azole drugs to *A. fumigatus*-infected mice
110 (23), but not to our knowledge in studies of *A. fumigatus* pathogenesis.

111 In this study we hypothesized that differentiated human PLB-985 neutrophil-like cells could serve as
112 model system to study the host-pathogenesis of *A. fumigatus* in a blood donor-independent manner. We tested
113 this hypothesis by defining the phagocytosis and intracellular trafficking of *A. fumigatus* conidia by PLB-985 cells,
114 the production of neutrophil extracellular traps, and the production of extracellular vesicles produced in response
115 to fungal infection. We find numerous similarities between this cell line and primary neutrophils that suggest
116 differentiated PLB-985 cells can serve as a tractable *in vitro* model system for further study of some aspects of *A.*
117 *fumigatus* pathogenesis.

118

119 **RESULTS**

120 **Differentiated PLB-985 neutrophil-like cells phagocytose opsonized *A. fumigatus* conidia.**

121 We set out to assess the feasibility of using *N,N*-dimethylformamide (DMF)-differentiated PLB-985 (dPLB) cells as
122 a model for neutrophil phagocytosis, NET production, and extracellular vesicles release in response to *A.*
123 *fumigatus* infection. Upon infection, neutrophils are known to rapidly phagocytose and process *A. fumigatus*
124 conidia. We therefore challenged dPLB cells with opsonized *A. fumigatus* resting conidia and assessed various
125 parameters of infection.

126 First, we determined the phagocytic capacity of PLB-985 cells using confocal laser scanning microscopy
127 following incubation of cells with fluorescein isothiocyanate (FITC)-labelled, opsonized conidia (green). We
128 observed that dPLBs were capable of phagocytosis, as evidenced by a phagosomal membrane surrounding the
129 conidia (**Fig. 1A**). A similar result was confirmed for primary human PMNs with this experimental setup (**Fig. S1A**).
130 Interestingly, dPLB cells only infrequently phagocytosed unopsonized conidia, whereas primary human
131 neutrophils indiscriminately phagocytosed both unopsonized and opsonized conidia (data not shown). To better
132 quantify phagocytosis, we analyzed 5,000 host cells post-infection by single-cell analysis using imaging flow
133 cytometry. For this we counterstained with calcofluor white (CFW; blue) to elucidate non-phagocytosed conidia
134 (**Fig. 1B and Fig. S1B to C**). Quantification of imaging flow cytometry data revealed that approximately 22% of
135 wild-type and 26% of non-pigmented Δ*pksP* conidia were phagocytosed by dPLBs after 2 hours, while
136 undifferentiated PLB-985 cells exhibited limited phagocytosis of both wild-type and non-pigmented conidia (**Fig.**
137 **1C**). As expected, these phagocytosis percentages were lower than those of primary human PMNs, which
138 phagocytosed 62% of wild-type and 54% of Δ*pksP* conidia after 2 hours and 90% of wild-type and 85% of Δ*pksP*
139 conidia after 4 hours of infection (**Fig. S1D**). We also measured the induction of cell damage following infection
140 using lactate dehydrogenase release assays and found levels below the limit of detection for dPLB cells after 2 and
141 4 hours of incubation (data not shown). To determine if infection also resulted in an activated immune response,
142 we measured proinflammatory cytokine levels by enzyme-linked immunosorbent assay (ELISA). Co-incubation of
143 dPLB cells with wild-type spores resulted in production of significantly increased levels of interleukin (IL)-8, but
144 not IL-1β after 24 hours of co-incubation, comparable to primary neutrophils at the corresponding earlier time
145 points (**Fig. 1D and Fig. S2**). Together, these results suggested that DMF-differentiated PLB-985 cells could serve
146 as a suitable model for *A. fumigatus* pathogenesis and warranted further investigation.

147

148 **Internalized *A. fumigatus* conidia are processed inside dPLB phagolysosomes.**

149 Following internalization of conidia by professional phagocytes like macrophages and neutrophils, conidia-
150 containing phagosomes fuse with lysosomes to acidify the compartment and aid in fungal killing. Numerous

151 additional enzymes are activated upon phagolysosomal acidification to degrade and digest the internalized fungal
152 conidia. The acidification and maturation of phagolysosomes are regulated by protein complexes assembled on
153 the phagolysosomal membrane, including lysosomal-associated membrane protein (LAMP)-1, 2, and 3; several
154 vacuolar ATPases (V-ATPases); Ras-related protein (RAB) 5 and 7; Flotillin 1 and 2; and numerous others (24). DHN-
155 melanin on the surface of conidia can interfere with these processes in alveolar macrophages, monocytes, and
156 primary neutrophils to delay fungal processing and phagolysosomal acidification (25). To test whether dPLB cells
157 process conidia similarly to primary human PMNs, we first stained the cells with LAMP-1, a general endocytic
158 marker on the membrane of phagolysosomes. LAMP-1 showed a clear signal around phagolysosomes of infected
159 cells (**Fig. 2A**), and the intensity of the signal did not differ between wild-type and *ΔpksP* conidia (**Fig. 2B**).
160 Furthermore, loading of dPLB cells with Lysotracker, a weak base that becomes fluorescent under acidic
161 conditions, showed that the *ΔpksP* conidia-containing phagosomes were significantly more acidified than those
162 containing wild-type conidia, revealing that DHN-melanin can also block the acidification process in the dPLB
163 model as well (**Fig. 2C to D**).
164 The interference of the acidification pathway in alveolar macrophages by fungal DHN-melanin occurs
165 through the inhibition of V-ATPase assembly (26, 27). This multiprotein complex plays a major role in lowering the
166 pH from 6 to <4.5 by pumping H^+ ions across the phagolysosomal membrane. Staining of the V-ATPase V1 subunit
167 in dPLB cells revealed that the percentage of recruitment to conidia-containing phagolysosomes was fairly similar
168 for wild-type and *ΔpksP* conidia (**Fig. S3A to B**), suggesting that other proton pumps may contribute to acidification
169 of these phagolysosomes in neutrophil-like cells. An additional defense mechanism for intra-phagosomal
170 degradation of pathogens occurs via reactive oxygen species (ROS) production. As expected, we observed dPLB
171 cells to be capable of producing ROS after staining with CellROX Orange (**Fig. S3C**), consistent with the literature
172 (28, 29).
173
174 ***A. fumigatus* triggers formation of NETs from dPLB cells.**
175 One defense mechanism employed by neutrophilic granulocytes to fight against pathogens is the formation of
176 NETs. These structures consist of condensed chromatin and various enzymes that are released into the
177 extracellular space and typically correlate with death of the cell (30). NETs contain several anti-fungal proteins,
178 which are responsible for the fungistatic effect against *A. fumigatus* hyphae (15). To test if dPLBs are also able to
179 form NETs in response to *A. fumigatus* and serve as a model for this pathway, we co-incubated dPLBs cells with
180 hyphae and stained for nucleic acid with 4′,6-diamidino-2-phenylindole (DAPI; **Fig. 3A**). As a positive control, we
181 induced NET formation using phorbol myristate acetate, a known trigger of NET formation in PLB-985 cells (**Fig.
182 3B**; (21, 31)). We observed the presence of histone H3 embedded in the DNA fibers and an association of NETs

183 with fungal hyphae (**Fig. 3B**). Taken together these results showed that *A. fumigatus* is able to trigger NET
184 formation in dPLB cells and that these NETs are specifically directed against the hyphae.
185
186 **dPLB cells produce extracellular vesicles in response to infection.**
187 Recently, a new defense mechanism from neutrophilic granulocytes was discovered, the production of
188 antimicrobial extracellular vesicles (32, 33). These small lipid-enclosed nanoparticles are released from primary
189 PMNs after contact with microorganisms and, in the case of *A. fumigatus* conidia, can inhibit fungal growth after
190 coincubation (10). This effect is likely due in part to their protein cargo, which consists of antimicrobial peptides
191 such as myeloperoxidase, azurocidin, and cathepsin G. To assess if dPLB cells can produce extracellular vesicles
192 spontaneously or in response to *A. fumigatus*, we incubated cells with or without conidia for 2 and 4 hours. Next,
193 we isolated extracellular vesicles using two different methods; first using a previously described differential
194 centrifugation-based approach (DC; (10)) that enriches for medium-sized extracellular vesicles and a second
195 approach that relies on size-exclusion chromatography (SEC) to purify a more selective population of smaller
196 extracellular vesicles. Using these methods, dPLB cells were observed to actively secrete extracellular vesicles over
197 time in a manner comparable to primary human PMNs (**Fig. 4A to B).** Using nanoparticle tracking analysis, we
198 observed the median size of particles to be around 200 nm, similar to extracellular vesicles derived from primary
199 neutrophils, a feature that was comparable between infection-derived and spontaneously released extracellular
200 vesicles (**Fig. 4C to D**).
201 We next compared the protein content of dPLB-derived extracellular vesicles isolated, at the 2 hours
202 timepoint, using each isolation method with and without fungal infection by LC-MS/MS-based proteomics
203 analysis. We were able to identify 1,984 unique proteins across all four samples (**Dataset S1**). The majority of
204 identified proteins (737 proteins) were found in all four samples (**Fig. 5A**). We expected that isolation using size-
205 exclusion chromatography would improve the quality of the isolated particles as has been shown previously (34),
206 and this was in fact the case. We observed an increase in extracellular vesicle markers like the tetraspanins CD63
207 and CD81, and tumor susceptibility gene 101 (TSG101), and a decrease in cytoplasmic proteins like calnexin (CANX;
208 **Table 1**).
209 Extracellular vesicles produced by primary PMNs in response to *A. fumigatus* infection are known to be
210 enriched for antimicrobial cargo proteins like azurocidin, cathepsin G, and defensin (10). In line, with the data
211 from primary neutrophils we found that dPLBs also contained many of the same proteins in both infection-derived
212 and spontaneously released extracellular vesicles (**Table 1**), as evidenced by an UpSetR plot showing overlapping
213 proteins cohorts (**Fig. S4;** (10)), although with some exceptions. For example, dPLBs appeared to lack defensin,
214 neutrophil elastase, and some histone proteins previously observed. Ultimately, improvements in LC-MS/MS

215 technology and the advantage of higher input amounts of extracellular vesicle protein using large amounts of
216 dPLB cells in culture resulted in significantly more proteins detected in the dataset provided here compared to
217 efforts using primary neutrophils (10), proving that dPLBs offer a scalable system for the elucidation of novel
218 mechanisms of neutrophil extracellular vesicle biology.
219
220 **dPLB extracellular vesicles produced against *A. fumigatus* limit fungal growth.**
221 The most compelling feature of infection-derived extracellular vesicles of human neutrophils is likely their
222 antifungal capacity, as we previously reported (10). We set out to determine if the extracellular vesicles produced
223 by dPLB cells in response to *A. fumigatus* opsonized conidia are antifungal to a mitochondrial-GFP reporter strain
224 used previously as a marker of fungal viability (35). First, we incubated the reporter strain with dPLB cells and
225 primary human PMNs and assessed the capacity of the cells to control infection. PMNs were capable of minimizing
226 fungal outgrowth after 22 hours, whereas dPLBs did not completely contain fungal growth (**Fig. 6A**). We then
227 assessed the antifungal capacity of the dPLB extracellular vesicles. For this experiment, extracellular vesicles from
228 equal numbers of dPLBs and primary human PMNs were isolated using differential centrifugation and found to be
229 antifungal against the mitochondrial-GFP reporter strain. This was evidenced by fragmentation of fungal
230 mitochondria after administration of extracellular vesicles to germinating conidia, which were allowed to
231 germinate for 6 hours prior to overnight incubation with extracellular vesicles, 3 mM H_2O_2 as a positive control,
232 or left untreated as a negative control (**Fig. 6B**). Although, the mitochondrial reporter clearly indicated
233 fragmentation, the extracellular vesicles from dPLB did appear to be in some cases less effective in limiting the
234 length development of the hyphae than those from primary PMNs. It is important to note that dPLBs produced
235 slightly fewer extracellular vesicles, which could potentially explain the decreased antifungal activity in these
236 assays (**Fig. 6B**). Additional representative images of dPLB-derived extracellular vesicles are shown to indicate the
237 spectrum of phenotypes observed for each experimental condition (**Fig. S5**)**.** Collectively, these results suggest
238 that dPLB infection-derived extracellular vesicles can limit *A. fumigatus* hyphal growth, similar in fashion to
239 primary human PMNs (10).
240
241 **MATERIALS AND METHODS**
242 **Fungal strains cultivation and opsonization.**
243 Cultivation of *A. fumigatus* strains CEA10 (Fungal Genetics Stock Center; A1163), CEA17 Δ*akuB*^{ku80} Δ*pksP* (36), and
244 AfS35/pJW103 (35) was performed on malt agar plates (Sigma-Aldrich) supplemented to a final concentration of
245 2% (wt/vol) agar for 5 days at 37 °C. Conidia were harvested in sterile, ultrafiltrated water, filtered through a 30-
246 µm pore filter (MACS, Miltenyi Biotec). Prior to confrontation with PLB-985 cells, conidia were opsonized with

247 normal human serum (Merck Millipore). Briefly, 900 µl of spore suspension was mixed with 100 µl of normal
248 human serum and incubated in a thermomixer at 37 °C for 30 min shaking at 500 rpm. The spore suspension was
249 washed three times by collecting spores *via* centrifugation at 1800 x *g* for 1 min at 4 °C and resuspending in fresh
250 PBS 1X. Following washing, spores were enumerated in a Thoma chamber in preparation for infection assays.
251
252 **Cell culture cultivation, differentiation, and infection.**
253 PLB-985 cells were maintained in Roswell Park Memorial Institute medium 1640 (RPMI; Gibco) supplemented with
254 10% (vol/vol) fetal bovine serum (FBS; HyClone, GE Life science), 100 U/ml penicillin-streptomycin antibiotic
255 solution (Lonza) and 2 mM UltraGlutamine (alanyl L-glutamine; Gibco). For differentiation into a neutrophilic
256 granulocyte cell type, 4×10^5 cells/ml were resuspended in supplemented RPMI medium containing 2.5% (vol/vol)
257 FBS and 0.5% DMF (Sigma-Aldrich) for 4 days at 37 °C with 5% (vol/vol) CO_2. On day 4, fresh differentiation medium
258 was added, and the cells were incubated for 3 additional days. On day 7, cells were collected, centrifuged at 300
259 x *g* for 5 min and then seeded in wells for experiments at the appropriate concentrations. The medium used for
260 all the assays was composed of RPMI supplemented with 1% (vol/vol) exosome-depleted FBS (Life Technologies
261 GmbH), 2 mM UltraGlutamine, and 0.5% (vol/vol) DMF.
262
263 **Isolation of human PMNs.** Fresh venous blood was drawn from adult healthy volunteers, aged 20 to 35 years,
264 after obtaining written consent. This study was approved by the Jena University Hospital Institutional Review
265 Board (approval number 5074-02/17) in agreement with the Declaration of Helsinki. Blood was collected in EDTA
266 BD Vacutainer tubes (BD Biosciences) and mixed with PBS 1X. 6 ml of this solution was carefully layered onto
267 (avoiding any mixing) 5 ml (1:1 vol/vol) of PolymorphPrep solution (Progen) and centrifuged 50 min at 500 x *g* for
268 gradient separation. After centrifugation the neutrophil layer was collected, mixed with an equal volume of PBS
269 0.5% and re-centrifuged for 15 min at 400 x *g*. To limit contamination of red blood cells, the pellet was lysed with
270 the ACK lysis buffer (Gibco) and centrifuged as before. The PMNs were finally re-suspended in RPMI medium
271 without phenol red (Thermo Fischer scientific) and after addition of Trypan blue counted with a Luna automated
272 cell counter (Logos biosystem). For each experiment the viability of neutrophils was $\geq$ 95%.
273
274 **Determination of cell viability.**
275 To assess cell viability after confrontation with *A. fumigatus* conidia, the release of LDH was determined using the
276 CyQUANT™ LDH cytotoxicity assay kit (Thermo Fisher Scientific) according to the manufacturer´s instruction. Cells
277 treated with *A. fumigatus* conidia with a multiplicity of infection (MOI) of 5 for 2 hours were tested for their LDH

278 activity, which was compared to the spontaneous LDH activity and the maximum LDH activity. Release of LDH was
279 below the limit of detection for all three independent biological replicates performed.
280
281 **Phagocytosis assays.**
282 To assess phagocytic ability, we used a combination of imaging flow cytometry and confocal fluorescence
283 microscopy. For both methods the conidia were first stained with fluorescein isothiocyanate (FITC) and then after
284 confrontation of dPLBs or primary neutrophils, counterstained with calcofluor white (CFW; Sigma -Aldrich). The
285 FITC solution was obtained by dissolving FITC powder (Sigma-Aldrich) in 5 mL of 0.1 M sodium carbonate (Na_2CO_3)
286 followed by filtration through a 0.22-µm pore size filter (Carl Roth). Afterwards 1 ml of this solution was mixed
287 with 500 µl of spore suspension and incubated for 30 min at 37 °C while shaking at 1000 rpm in the dark. The
288 spores were then pelleted and washed three times with PBS 1X with 0.001% (vol/vol) Tween 20 (Carl Roth). During
289 the last washing step Tween was removed to avoid residual detergent in the samples (25, 37). Before counting,
290 the conidia were opsonized following the protocol described above. They were then added to the cells and co-
291 incubated for 2 and 4 hours at 37 °C with 5% (vol/vol) CO_2. At the end of each time point CFW was added to a final
292 concentration of 1 µg/ml and incubated for 1 min. Afterwards the cell suspension was transferred to
293 microcentrifuge tubes, centrifuged at 600 x *g* for 2 min at 4 °C and washed with PBS 1X twice. After discarding the
294 supernatant, the pellet was fixed with 150 µL of 3.7% (vol/vol) formaldehyde in PBS at room temperature for 15
295 min and subsequently washed again as described above. For imaging flow cytometry measurements, the cells
296 were resuspended in 150 µL of PBS 1X and analyzed immediately or stored at 4 °C for no more than 24 hours. Four
297 independent experiments were performed and for each replicate 5000 cells were analyzed using the ImageStream
298 X Mark II (Luminex). A 488 nm laser was used to detect FITC staining and a 405 nm laser for the CFW. The laser
299 voltage was adjusted depending on the sample. For wild-type conidia, we used 10 mW of 488 nm laser and 2 mW
300 for the 405 nm laser, and for Δ*pksP* conidia 1 and 2 mW of the respective lasers. The fluorescence intensities of
301 the samples were compensated and analyzed with the IDEAS software (Luminex). An example of the gating
302 strategy used for analysis can be found in the supplement files (**Fig. S1B to C**). For the fluorescence microscopy
303 analysis, cells were seeded in 8-well µ-slides (Ibidi) and visualized using a Zeiss LSM 780 confocal microscope (Carl
304 Zeiss) from at least three biological replicates as described above.
305
306 **Immunofluorescence assays.**
307 For immunofluorescence, cells were allowed to adhere in a 24-well plate with poly-L-lysine-coated glass coverslips
308 for 1 hour (Merck). After infection with labelled *A. fumigatus* spores and incubation for the noted times, cells were
309 fixed using 3.7% (vol/vol) formaldehyde in PBS for 10 min, rinsed three times with PBS 1X, permeabilized for 15

310 min using 0.1% (vol/vol) Triton X-100 in PBS 1X or 0.1% (wt/vol) saponin in PBS 1X, and then blocked for 30 min
311 with 2% (wt/vol) bovine serum albumin (BSA). After permeabilization, washed cells were incubated with primary
312 rabbit anti-Lamp-1 antibody (Abcam 24170, 1:100 dilution), anti-V-ATPase V1 subunit antibody (Abcam 73404,
313 1:100 dilution), or anti-Histone H3 (Cell signaling DIH2, 1:200 dilution) antibody in 1% (wt/vol) BSA in PBS 1X,
314 followed by incubation with secondary goat anti-rabbit IgG antibody DyLight 633 (Thermo Fisher Scientific). The
315 glass cover slips were mounted onto microscopy slides and visualized using a Zeiss LSM 780 confocal microscope
316 (Carl Zeiss). LAMP-1 recruitment was quantified by comparing the positive signal from stained phagolysosomes to
317 non-stained phagolysosomes.
318
319 **Reactive oxygen species measurements.**
320 ROS production was detected in dPLB cells by seeding cells in 8-well µ-slides (Ibidi) coated with poly-L-lysine
321 followed by infection with *A. fumigatus conidia* at an MOI of 5 for either 2 or 4 hours. CellROX® Orange Reagent
322 (Thermo Fisher Scientific) was added 30 minutes prior the end of the infection time points, and ROS production
323 was imaged using a Zeiss LSM 780 confocal microscope (Carl-Zeiss) for fluorescent intensity.
324
325 **Cytokine measurement.**
326 For the detection of IL-8 and IL-1β, $2x10^5$ dPLB cells or primary neutrophils were seeded in 24-well plates. After
327 addition of conidia at a MOI of 5, plates were incubated at 37 °C with 5% (vol/vol) CO_2 for 2, 4, or 6 hours. An
328 additional 24-hour timepoint was included for dPLB cells. As a positive control, cells were treated with 5 µg/mL of
329 lipopolysaccharide (LPS; Sigma-Aldrich L4516). At the appropriate end point, samples were collected, centrifuged
330 at 300 x *g* for 5 min to remove cell debris, and frozen at -20°C and analyzed within 3 days. Cytokines were
331 measured using human ELISA Max deluxe kits (BioLegend) according to the manufacturer´s instruction.
332
333 **Acidification assays.**
334 Acidification assays were performed as mentioned previously (27). Briefly, the cells were incubated with 50 nM
335 lysotracker DND-99 (Thermo Fisher Scientific) for 1 hour prior to infection. After that, FITC-labeled conidia were
336 added to the cells for 2 or 4 hours and imaged using Zeiss LSM 780 confocal microscope (Carl Zeiss). For
337 quantification, 200 conidia-containing phagolysosomes were counted and evaluated for acidification. The values
338 represent the mean ± SD of three separate experiments.
339
340 **Extracellular vesicle isolation.**

341 After infection with *A. fumigatus* the supernatant of dPLB cells was collected, and extracellular vesicles were
342 isolated using two different methods: a differential centrifugation-based approach or a size exclusion
343 chromatography-based approach. The first method was described previously for the isolation of neutrophil-
344 derived extracellular vesicles (10, 32). In both approaches samples were centrifuged at 3000 x *g* for 15 min at 4 °C
345 and then filtered through 5-µm pore size filters (Carl Roth). In the first method, samples were then centrifuged at
346 19,500 x *g* for 20 min at 4 °C to collect extracellular vesicles. For the second approach, the clarified filtrate was
347 concentrated using Amicon Ultra-15 centrifugal filters (Merck) with a molecular mass cut-off (MWCO) of 100 kDa
348 for 10 min at 4 °C and 3220 *x g* and finally loaded on size-exclusion chromatography qEV 70 nm columns (Izon).
349 After discarding the 3 mL void volume, 1.5 mL of extracellular vesicle sample were collected and measured. When
350 necessary, extracellular vesicles were further concentrated using 10 kDa cutoff Amicon Ultra-0.5 ml filters (Merck).
351 Extracellular vesicles were used fresh for most of the downstream experiments except for proteomic analysis
352 where they were frozen at -20 °C.
353
354 **Nanoparticle tracking analysis.**
355 Particle concentration and size distribution were analyzed using a nanoparticle tracking analysis (NTA) NS300
356 device with a 650 nm laser (Malvern Instruments Ltd). Fresh samples were measured with a constant flow rate of
357 20 and a temperature set to 25 °C. Five 60-second videos were recorded with a camera level of 11. Videos were
358 then analyzed with the NTA 3.2.16 software using a detection threshold of 4.
359
360 **Protein preparation for LC-MS/MS.**
361 After isolation as described above, extracellular vesicles were delipidated as described previously (10) using the
362 protein precipitation protocol of Wessel and Flügge (38). Delipidated extracellular vesicles were resolubilized in
363 100 µl of 50 mM triethyl ammonium bicarbonate (TEAB) in 1:1 (vol/vol) trifluoroethanol/water. For reduction of
364 cysteine thiols, the solution was mixed with 10 mM Tris(2-carboxyethyl) phosphine and alkylated with 12.5 mM
365 chloroacetamide at 70 °C for 30 min in the dark. Proteins were digested for 18 hours at 37 °C with trypsin/LysC
366 mix (Promega) at a protein-to-protease ratio of 25:1. Tryptic peptides were first completely evaporated using a
367 vacuum concentrator (Eppendorf) and then resolubilized in 0.05% (vol/vol) trifluoroacetic acid (TFA) in 2:98
368 (vol/vol) acetonitrile/water. Finally, the samples were filtered through Ultrafree-MC Hydrophilic PTFE membrane
369 (0.2-µm pore size) spin filters (Millipore) and stored at -20 °C until measurement. Each sample was measured in
370 triplicate (3 analytical replicates of 3 biological replicates) as follows.
371
372 **LC-MS/MS analysis.**

373 LC-MS/MS analysis was performed on an Ultimate 3000 nano RSLC system connected to a QExactive HF mass
374 spectrometer (both Thermo Fisher Scientific). Peptide trapping for 5 min on an Acclaim Pep Map 100 column (2
375 cm x 75 µm, 3 µm) at 5 µL/min was followed by separation on an analytical Acclaim Pep Map RSLC nano column
376 (50 cm x 75 µm, 2µm). Mobile phase gradient elution of eluent A (0.1% (vol/vol) formic acid in water) mixed with
377 eluent B (0.1% (vol/vol) formic acid in 90/10 acetonitrile/water) was performed as follows: 0 min at 4% B, 30 min
378 at 12% B, 75 min at 30% B, 85 min at 50% B, 90-95 min at 96% B, 95.1-120 min at 4% B.
379 Positively charged ions were generated at spray voltage of 2.2 kV using a stainless-steel emitter attached
380 to the Nanospray Flex Ion Source (Thermo Fisher Scientific). The quadrupole/orbitrap instrument was operated in
381 Full MS / data dependent MS2 (Top15) mode. Precursor ions were monitored at m/z 300-1500 at a resolution of
382 120,000 FWHM (full width at half maximum) using a maximum injection time (ITmax) of 120 ms and an AGC
383 (automatic gain control) target of $3x10^6$. Precursor ions with a charge state of z=2-5 were filtered at an isolation
384 width of m/z 1.6 amu for further HCD fragmentation at 27% normalized collision energy (NCE). MS2 ions were
385 scanned at 15,000 FWHM (ITmax=100 ms, AGC= $2x10^5$). Dynamic exclusion of precursor ions was set to 25 s and
386 the underfill ratio was set to 1.0%. The LC-MS/MS instrument was controlled by Chromeleon 7.2, QExactive HF
387 Tune 2.8 and Xcalibur 4.0 software.
388
389 **Database search and data analysis**
390 Tandem mass spectra were searched against the UniProt database of *Homo sapiens*
391 (https://www.uniprot.org/proteomes/UP000005640; 2021/05/17) and *Neosartorya fumigata*
392 (https://www.uniprot.org/proteomes/UP000002530; 2021/05/17) using Proteome Discoverer (PD) 2.4 (Thermo)
393 and the algorithms of Mascot 2.4.1 (Matrix Science), Sequest HT (version of PD2.2), MS Amanda 2.0, and MS
394 Fragger 3.2. Two missed cleavages were allowed for the tryptic digestion. The precursor mass tolerance was set
395 to 10 ppm and the fragment mass tolerance was set to 0.02 Da. Modifications were defined as dynamic Met
396 oxidation, and protein N-term acetylation with and without methionine-loss as well as static Cys
397 carbamidomethylation. A strict false discovery rate (FDR) < 1% (peptide and protein level) were required for
398 positive protein hits. If only 1 peptide per protein has been identified the hit was accepted if the Mascot score
399 was >30 or the MS Amanda score was >300 or the Sequest score was >4 or the MS Fragger score was >8. The
400 Percolator node of PD2.4 and a reverse decoy database was used for qvalue validation of spectral matches. Only
401 rank 1 proteins and peptides of the top scored proteins were counted. Label-free protein quantification was based
402 on the Minora algorithm of PD2.2 using a signal-to-noise ratio >5. Imputation of missing quan values was applied
403 by setting the abundance to 75% of the lowest abundance identified for each sample. Normalization was based
404 on a replicate median total peptide sum approach, which was calculated based on the sum of all identified peptide

405 abundance values per replicate sample. The sums of each of the three replicates from the four sample groups
406 were used to calculate median values. Normalization factors were calculated by dividing median values of the
407 respective sample group by the abundance sum of each sample. Normalization factors were multiplied with single
408 protein abundance values of each replicate/sample. The p-values are based on a Student`s t-test. Ratio-adjusted
409 p-values were calculated by dividing p-values with the log4ratio of the protein abundance levels. Significant
410 differences in protein abundance were defined when the following three requirements were reached: At least a
411 4-fold change in abundance (up and down), a ratio-adjusted p-value <0.05, and at least identified in 2 of 3
412 replicates of the sample group with the highest abundance. Intersection plots were created using the UpSetR
413 package (39) and only include proteins that were detected in at least two replicates of a given sample. Volcano
414 plots were created using ggplot2 in R using the replicate median total peptide sum normalized (RMN) data for all
415 proteins detected in **Dataset S1**.

416 **Fungal mitochondrial reporter inhibition assay**

417 To characterize growth inhibition and killing of hyphae by fungal-induced extracellular vesicles an *A. fumigatus*
418 strain expressing a mitochondrial GFP reporter (AfS35/pJW103; (35)) has been used as described previously (10).
419 Extracellular vesicles produced by $1x10^7$ dPLB cells or PMNs were isolated and co-incubated with the reporter
420 strain. After 16 hours of incubation samples were stained with CFW and images were taken using Zeiss LSM 780
421 confocal microscope (Carl Zeiss).

422

423 **Data availability**

424 The mass spectrometry proteomics data have been deposited to the ProteomeXchange Consortium via the PRIDE
425 partner repository (40) with the dataset identifier PXD027032.

426

427 **Statistical Analysis.** Data were plotted and statistically analyzed using GraphPad Prism software 5.0 (GraphPad
428 Software) unless otherwise noted. The Student's t test was used for significance testing when comparing two
429 groups. Differences between the groups were considered significant at a P value of <0.05. Throughout the article,
430 significance is denoted as follows: *, P = <0.05; **, P = <0.01, ***, P = <0.001; ns, nonsignificant.

431

432 **Ethics Statement.** Peripheral human blood was collected from healthy volunteers only after written informed
433 consent was provided. The study was conducted in accordance with the Declaration of Helsinki and approved by
434 the Ethics Committee of the University Hospital Jena (approval number 5074-02/17).

435

436 **DISCUSSION**

437 Neutrophils are critical players in the immune response to fungal pathogens stemming from their numerous
438 antimicrobial capacities (10, 41). To study neutrophil functions, numerous cell lines that model these abilities *in*
439 *vitro* have been considered with limited success. The most promising remains the HL-60 leukemia cell line and
440 PLB-985 sublineage, which have been used as models for aspergillosis and bacterial killing (21-23, 28). In the
441 present study, we analyze different aspects of the interaction between DMF-differentiated PLB-985 myeloid cells
442 and the fungus *A. fumigatus* for the first time, making frequent comparisons with data from primary neutrophils.

443 Primary neutrophils are capable of phagocytosing and processing *A. fumigatus* conidia, features that were
444 maintained in dPLB cells. As expected for cultured cells, the observed phagocytosis rate of *A. fumigatus* conidia
445 by dPLB cells was lower than that of primary human PMNs. It is possible that additional differentiation methods
446 will ultimately reveal higher rates of phagocytosis, as PLB-985 cells differentiated with DMF are known to exhibit
447 lower phagocytic activity than cells differentiated with dimethyl sulfoxide (42). In terms of cytokine release, we
448 observed increased release of IL-8 from dPLBs after infection with *A. fumigatus* opsonized conidia, but not IL-1β,
449 consistent with our observations in human PMNs. These results are also in agreement with those collected from
450 primary PMNs co-incubated with L-ficolin opsonized conidia for 8 hours, where secretion of IL-8 was also much
451 higher than IL-1β (43).

452 We next stained dPLB cells for the endosomal marker LAMP-1 and measured the acidification of the
453 phagolysosomes via Lysotracker to assess intracellular processing of fungal conidia. These experiments confirmed
454 that around 20% of wild-type conidia are completely internalized inside the phagosomes and that lysosomal fusion
455 occurs as a next step of conidial processing. Interestingly, and as already demonstrated for primary monocytes
456 and neutrophils (25), melanized conidia showed less acidification around the phagolysosomal membrane than the
457 mutant lacking DHN-melanin. This effect in monocytes is caused by inhibition of V-ATPase assembly. Surprisingly,
458 staining for the V1 subunit of the V-ATPase did not reveal a significant difference between the wild-type and Δ*pksP*
459 strains in dPLB cells as has been observed in other cell systems. These results suggest that neutrophils potentially
460 employ additional mechanisms to acidify phagolysosomes in neutrophilic granulocytes after *A. fumigatus*
461 infection or that the methods used were not sufficiently sensitive to detect slight differences in acidification.
462 Together, these results suggest that dPLBs can serve as an intriguing model to study various aspects of neutrophil
463 phagocytosis and intracellular processing in a more tractable *in vitro* model system.

464 A conidium that escapes phagocytosis can sometimes germinate into a hypha, a morphotype that is much
465 more difficult to eliminate and requires the antifungal activity of neutrophils. One mechanism that aids in control
466 of *A. fumigatus* hyphae is the release of fungistatic NETs composed of DNA and antimicrobial proteins. By staining
467 for extracellular DNA and NET constituent histone H3, we could clearly show that dPLB cells also produce NETs in
468 response to *A. fumigatus* hyphae, comparable to primary human PMNs and in agreement with other studies
469 challenging dPLBs with bacterial pathogens (21, 22).

470 Production of extracellular vesicles from primary neutrophils co-incubated with *Aspergillus* conidia or
471 bacteria like *Staphylococcus aureus* is an important defense strategy against microorganisms (10, 32). We found
472 that dPLB cells were also able to generate comparable populations of extracellular vesicles to PMNs upon contact
473 with opsonized conidia. Accumulation of extracellular vesicles of approximately 200 nm in diameter was observed
474 over time, independently of the isolation method we applied. Proteomic analysis revealed that by using a size-
475 exclusion chromatography-based isolation approach, the extracellular vesicles population could be enriched for
476 extracellular vesicle marker proteins like CD63, CD81, and TSG101. We observed that the samples obtained by
477 this method had a higher abundance of proteins and showed more differences between the spontaneously
478 released and infection-derived extracellular vesicles. In particular, infection-derived extracellular vesicles were
479 enriched in immunoglobulins and complement factors when compared to spontaneously released vesicles. These
480 serum proteins may be introduced to the infection system during opsonization of the fungal conidia despite
481 thorough washing. It remains unclear whether these immunoglobulins and complement factors play an important
482 role in extracellular vesicle biology during *A. fumigatus* infection. As a hint for such a role, the association of
483 immunoglobulins and complement proteins was shown previously to be important in systemic lupus
484 erythematosus (SLE) disease, where extracellular vesicles with immunoglobulin cargo could act as immune
485 complexes to mediate inflammation (44, 45).

486 In the proteomic analysis of extracellular vesicles derived from primary neutrophils infected with *A.*
487 *fumigatus*, several antimicrobial peptides, such as cathepsin G and azurocidin, were detected (10). Co-incubation
488 of these extracellular vesicles from primary neutrophils with fungal hyphae arrested growth, which was confirmed
489 in this study. Using dPLB cells, we identified extracellular vesicles containing cathepsin G and azurocidin; however,
490 the distribution remained relatively equal between spontaneously released and infection-derived extracellular
491 vesicles. We suspect that this is due to the differentiation procedure of dPLB cells with DMF, which provides a
492 mild inflammatory stimulus. Nevertheless, we observed mitochondrial damage in hyphae treated with infection-
493 derived but not spontaneously released extracellular vesicles. We can postulate several reasons for this result.
494 First, it is possible that immunoglobulins are playing a role in targeting extracellular vesicles to fungal hyphae. In
495 this case, the protein cargo may be the same, but targeting would be inefficient in spontaneously released

496 extracellular vesicles. Of note, opsonization of the bacterial pathogen *Staphylococcus aureus* was not found to
497 influence the antimicrobial capacity of neutrophil-derived extracellular vesicles (32). A second option is that
498 additional extracellular vesicle cargo molecules such as RNA or lipids may play a role in the antifungal activity. It
499 has been shown in many instances that extracellular vesicles can contain small RNAs that exert distinct functions
500 during infection, especially in regard to plant fungal pathogens (46, 47). We believe that a combination of factors
501 is likely involved in the antifungal effect of extracellular vesicles.

502 Part of the explanation may also come from similarities between neutrophilic granules and extracellular
503 vesicles. Granules and extracellular vesicles are distinct cellular features, but do share some biogenesis pathways
504 and cargo molecules. For example, the azurophilic granules contain myeloperoxidase to aid in pathogen killing in
505 the endocytic pathway via fusion of the granules to pathogen-containing phagosomes (48), but myeloperoxidase
506 is also released in a CD63-negative population of extracellular vesicles known as microvesicles (49). Based on the
507 proteomics analysis of this study, as well as our previous work (10), it seems possible that microvesicle-cargo
508 proteins like myeloperoxidase contribute at least in part to the antifungal activity. However, the presence of
509 myeloperoxidase in spontaneously released extracellular vesicles and the lack of susceptibility of patients lacking
510 myeloperoxidase to fungal infections (50) hint that other factors are also involved. Besides, the shared marker
511 protein CD63 nicely highlights another link between granules and extracellular vesicles, the shared biogenesis
512 from multivesicular bodies of azurophilic granules and the extracellular vesicle subset called exosomes (51).

513 In conclusion our results suggest that DMF-differentiated PLB-985 cells can be used as a model to study
514 aspects of the interaction of the human pathogenic fungus *A. fumigatus* with neutrophilic granulocytes. Although
515 they will never substitute for all experiments with neutrophils, we do believe that this system will serve as a useful
516 tool for the genetic dissection of *A. fumigatus* pathogenesis in the future.

517

518 **ACKNOWLEDGEMENTS**

519 We would like to thank Johannes Wagener for providing the *A. fumigatus* mitochondrial GFP reporter strain. We
520 also thank Natascha Wilker for excellent technical assistance. The work presented here was generously
521 supported by the Deutsche Forschungsgemeinschaft (DFG)-funded Collaborative Research Center/Transregio
522 FungiNet 124 'Pathogenic fungi and their human host: Networks of Interaction' (210879364, project A1 and Z2),
523 the DFG-funded ANR project (316898429, project AfuInf), and by the Federal Ministry for Education and
524 Research (BMBF: https://www.bmbf.de/), Germany, Project FKZ 01K12012 "RFIN – RNA-Biologie von
525 Pilzinfektionen." The authors declare no conflicts of interest.

526

527

528 **REFERENCES**

529 1. Brown GD, Denning DW, Gow NA, Levitz SM, Netea MG, White TC. 2012. Hidden killers: human fungal
530 infections. Sci Transl Med 4:165rv13.
531 2. Schmiedel Y, Zimmerli S. 2016. Common invasive fungal diseases: an overview of invasive candidiasis,
532 aspergillosis, cryptococcosis, and Pneumocystis pneumonia. Swiss Med Wkly 146:w14281.
533 3. Latge JP, Chamilos G. 2019. *Aspergillus fumigatus* and Aspergillosis in 2019. Clin Microbiol Rev 33.
534 4. Nasir N, Farooqi J, Mahmood SF, Jabeen K. 2020. COVID-19-associated pulmonary aspergillosis (CAPA) in
535 patients admitted with severe COVID-19 pneumonia: An observational study from Pakistan. Mycoses
536 63:766-770.
537 5. Salmanton-Garcia J, Sprute R, Stemler J, Bartoletti M, Dupont D, Valerio M, Garcia-Vidal C, Falces-Romero
538 I, Machado M, de la Villa S, Schroeder M, Hoyo I, Hanses F, Ferreira-Paim K, Giacobbe DR, Meis JF,
539 Gangneux JP, Rodriguez-Guardado A, Antinori S, Sal E, Malaj X, Seidel D, Cornely OA, Koehler P,
540 FungiScope European Confederation of Medical Mycology/The International Society for H, Animal
541 Mycology Working G. 2021. COVID-19-Associated Pulmonary Aspergillosis, March-August 2020. Emerg
542 Infect Dis 27:1077-1086.
543 6. Rivera A, Hohl TM, Collins N, Leiner I, Gallegos A, Saijo S, Coward JW, Iwakura Y, Pamer EG. 2011. Dectin-
544 1 diversifies *Aspergillus fumigatus*-specific T cell responses by inhibiting T helper type 1 CD4 T cell
545 differentiation. J Exp Med 208:369-81.
546 7. Brakhage AA, Langfelder K. 2002. Menacing mold: the molecular biology of *Aspergillus fumigatus*. Annu
547 Rev Microbiol 56:433-55.
548 8. Drummond RA, Gaffen SL, Hise AG, Brown GD. 2014. Innate Defense against Fungal Pathogens. Cold Spring
549 Harb Perspect Med 5.
550 9. Mircescu MM, Lipuma L, van Rooijen N, Pamer EG, Hohl TM. 2009. Essential role for neutrophils but not
551 alveolar macrophages at early time points following *Aspergillus fumigatus* infection. J Infect Dis 200:647-
552 56.
553 10. Shopova IA, Belyaev I, Dasari P, Jahreis S, Stroe MC, Cseresnyes Z, Zimmermann AK, Medyukhina A,
554 Svensson CM, Kruger T, Szeifert V, Nietzsche S, Conrad T, Blango MG, Kniemeyer O, von Lilienfeld-Toal M,
555 Zipfel PF, Ligeti E, Figge MT, Brakhage AA. 2020. Human Neutrophils Produce Antifungal Extracellular
556 Vesicles against *Aspergillus fumigatus*. mBio 11.
557 11. McCormick A, Heesemann L, Wagener J, Marcos V, Hartl D, Loeffler J, Heesemann J, Ebel F. 2010. NETs
558 formed by human neutrophils inhibit growth of the pathogenic mold *Aspergillus fumigatus*. Microbes
559 Infect 12:928-36.
560 12. Brogan TD. 1964. Effect of Complement and of the Carbohydrate Components of Sputum on Phagocytosis
561 by Human Polymorphonuclear Leucocytes. Immunology 7:626-38.
562 13. Pazhakh V, Ellett F, Croker BA, O'Donnell JA, Pase L, Schulze KE, Greulich RS, Gupta A, Reyes-Aldasoro CC,
563 Andrianopoulos A, Lieschke GJ. 2019. beta-glucan-dependent shuttling of conidia from neutrophils to
564 macrophages occurs during fungal infection establishment. PLoS Biol 17:e3000113.
565 14. Silva JC, Rodrigues NC, Thompson-Souza GA, Muniz VS, Neves JS, Figueiredo RT. 2020. Mac-1 triggers
566 neutrophil DNA extracellular trap formation to *Aspergillus fumigatus* independently of PAD4 histone
567 citrullination. J Leukoc Biol 107:69-83.
568 15. Bruns S, Kniemeyer O, Hasenberg M, Aimanianda V, Nietzsche S, Thywissen A, Jeron A, Latge JP, Brakhage
569 AA, Gunzer M. 2010. Production of extracellular traps against *Aspergillus fumigatus* in vitro and in infected
570 lung tissue is dependent on invading neutrophils and influenced by hydrophobin RodA. PLoS Pathog
571 6:e1000873.
572 16. Clark HL, Abbondante S, Minns MS, Greenberg EN, Sun Y, Pearlman E. 2018. Protein Deiminase 4 and CR3
573 Regulate *Aspergillus fumigatus* and beta-Glucan-Induced Neutrophil Extracellular Trap Formation, but
574 Hyphal Killing Is Dependent Only on CR3. Front Immunol 9:1182.

575 17. Zarember KA, Sugui JA, Chang YC, Kwon-Chung KJ, Gallin JI. 2007. Human polymorphonuclear leukocytes
576 inhibit *Aspergillus fumigatus* conidial growth by lactoferrin-mediated iron depletion. J Immunol 178:6367-
577 73.
578 18. Gazendam RP, van Hamme JL, Tool AT, Hoogenboezem M, van den Berg JM, Prins JM, Vitkov L, van de
579 Veerdonk FL, van den Berg TK, Roos D, Kuijpers TW. 2016. Human Neutrophils Use Different Mechanisms
580 To Kill *Aspergillus fumigatus* Conidia and Hyphae: Evidence from Phagocyte Defects. J Immunol 196:1272-
581 83.
582 19. Lahoz-Beneytez J, Elemans M, Zhang Y, Ahmed R, Salam A, Block M, Niederalt C, Asquith B, Macallan D.
583 2016. Human neutrophil kinetics: modeling of stable isotope labeling data supports short blood neutrophil
584 half-lives. Blood 127:3431-8.
585 20. Blanter M, Gouwy M, Struyf S. 2021. Studying Neutrophil Function in vitro: Cell Models and Environmental
586 Factors. J Inflamm Res 14:141-162.
587 21. Marin-Esteban V, Turbica I, Dufour G, Semiramoth N, Gleizes A, Gorges R, Beau I, Servin AL, Lievin-Le Moal
588 V, Sandre C, Chollet-Martin S. 2012. Afa/Dr diffusely adhering *Escherichia coli* strain C1845 induces
589 neutrophil extracellular traps that kill bacteria and damage human enterocyte-like cells. Infect Immun
590 80:1891-9.
591 22. Amulic B, Knackstedt SL, Abu Abed U, Deigendesch N, Harbort CJ, Caffrey BE, Brinkmann V, Heppner FL,
592 Hinds PW, Zychlinsky A. 2017. Cell-Cycle Proteins Control Production of Neutrophil Extracellular Traps.
593 Developmental Cell 43:449-462.e5.
594 23. Baistrocchi SR, Lee MJ, Lehoux M, Ralph B, Snarr BD, Robitaille R, Sheppard DC. 2017. Posaconazole-
595 Loaded Leukocytes as a Novel Treatment Strategy Targeting Invasive Pulmonary Aspergillosis. J Infect Dis
596 215:1734-1741.
597 24. Goyette G, Boulais J, Carruthers NJ, Landry CR, Jutras I, Duclos S, Dermine JF, Michnick SW, LaBoissiere S,
598 Lajoie G, Barreiro L, Thibault P, Desjardins M. 2012. Proteomic characterization of phagosomal membrane
599 microdomains during phagolysosome biogenesis and evolution. Mol Cell Proteomics 11:1365-77.
600 25. Thywissen A, Heinekamp T, Dahse HM, Schmaler-Ripcke J, Nietzsche S, Zipfel PF, Brakhage AA. 2011.
601 Conidial Dihydroxynaphthalene Melanin of the Human Pathogenic Fungus *Aspergillus fumigatus*
602 Interferes with the Host Endocytosis Pathway. Front Microbiol 2:96.
603 26. Heinekamp T, Schmidt H, Lapp K, Pahtz V, Shopova I, Koster-Eiserfunke N, Kruger T, Kniemeyer O,
604 Brakhage AA. 2015. Interference of *Aspergillus fumigatus* with the immune response. Semin
605 Immunopathol 37:141-52.
606 27. Schmidt F, Thywissen A, Goldmann M, Cunha C, Cseresnyes Z, Schmidt H, Rafiq M, Galiani S, Graler MH,
607 Chamilos G, Lacerda JF, Campos A, Jr., Eggeling C, Figge MT, Heinekamp T, Filler SG, Carvalho A, Brakhage
608 AA. 2020. Flotillin-Dependent Membrane Microdomains Are Required for Functional Phagolysosomes
609 against Fungal Infections. Cell Rep 32:108017.
610 28. Pedruzzi E, Fay M, Elbim C, Gaudry M, Gougerot-Pocidalo MA. 2002. Differentiation of PLB-985 myeloid
611 cells into mature neutrophils, shown by degranulation of terminally differentiated compartments in
612 response to N-formyl peptide and priming of superoxide anion production by granulocyte-macrophage
613 colony-stimulating factor. Br J Haematol 117:719-26.
614 29. Volk AP, Barber BM, Goss KL, Ruff JG, Heise CK, Hook JS, Moreland JG. 2011. Priming of neutrophils and
615 differentiated PLB-985 cells by pathophysiological concentrations of TNF-alpha is partially oxygen
616 dependent. J Innate Immun 3:298-314.
617 30. Branzk N, Papayannopoulos V. 2013. Molecular mechanisms regulating NETosis in infection and disease.
618 Semin Immunopathol 35:513-30.
619 31. Xie K, Varatnitskaya M, Maghnouj A, Bader V, Winklhofer KF, Hahn S, Leichert LI. 2020. Activation leads to
620 a significant shift in the intracellular redox homeostasis of neutrophil-like cells. Redox Biol 28:101344.

621 32. Timar CI, Lorincz AM, Csepanyi-Komi R, Valyi-Nagy A, Nagy G, Buzas EI, Ivanyi Z, Kittel A, Powell DW,
622 McLeish KR, Ligeti E. 2013. Antibacterial effect of microvesicles released from human neutrophilic
623 granulocytes. Blood 121:510-8.
624 33. Brakhage AA, K. ZA, Rivieccio F, Visser C, Blango MG. 2021. Host-derived extracellular vesicles for
625 antimicrobial defense. microLife doi:10.1093/femsml/uqab003/6228840.
626 34. Lane RE, Korbie D, Trau M, Hill MM. 2019. Optimizing Size Exclusion Chromatography for Extracellular
627 Vesicle Enrichment and Proteomic Analysis from Clinically Relevant Samples. Proteomics 19:e1800156.
628 35. Ruf D, Brantl V, Wagener J. 2018. Mitochondrial Fragmentation in *Aspergillus fumigatus* as Early Marker
629 of Granulocyte Killing Activity. Front Cell Infect Microbiol 8:128.
630 36. Hillmann F, Novohradska S, Mattern DJ, Forberger T, Heinekamp T, Westermann M, Winckler T, Brakhage
631 AA. 2015. Virulence determinants of the human pathogenic fungus *Aspergillus fumigatus* protect against
632 soil amoeba predation. Environ Microbiol 17:2858-69.
633 37. Kraibooj K, Schoeler H, Svensson CM, Brakhage AA, Figge MT. 2015. Automated quantification of the
634 phagocytosis of *Aspergillus fumigatus* conidia by a novel image analysis algorithm. Front Microbiol 6:549.
635 38. Wessel D, Flugge UI. 1984. A method for the quantitative recovery of protein in dilute solution in the
636 presence of detergents and lipids. Anal Biochem 138:141-3.
637 39. Lex A, Gehlenborg N, Strobelt H, Vuillemot R, Pfister H. 2014. UpSet: Visualization of Intersecting Sets.
638 IEEE Trans Vis Comput Graph 20:1983-92.
639 40. Perez-Riverol Y, Xu QW, Wang R, Uszkoreit J, Griss J, Sanchez A, Reisinger F, Csordas A, Ternent T, Del-
640 Toro N, Dianes JA, Eisenacher M, Hermjakob H, Vizcaino JA. 2016. PRIDE Inspector Toolsuite: Moving
641 Toward a Universal Visualization Tool for Proteomics Data Standard Formats and Quality Assessment of
642 ProteomeXchange Datasets. Mol Cell Proteomics 15:305-17.
643 41. Feldmesser M. 2006. Role of neutrophils in invasive aspergillosis. Infect Immun 74:6514-6.
644 42. Pivot-Pajot C, Chouinard FC, El Azreq MA, Harbour D, Bourgoin SG. 2010. Characterisation of
645 degranulation and phagocytic capacity of a human neutrophilic cellular model, PLB-985 cells.
646 Immunobiology 215:38-52.
647 43. Bidula S, Sexton DW, Schelenz S. 2016. Serum opsonin ficolin-A enhances host-fungal interactions and
648 modulates cytokine expression from human monocyte-derived macrophages and neutrophils following
649 *Aspergillus fumigatus* challenge. Med Microbiol Immunol 205:133-42.
650 44. Buzas EI, Toth EA, Sodar BW, Szabo-Taylor KE. 2018. Molecular interactions at the surface of extracellular
651 vesicles. Semin Immunopathol 40:453-464.
652 45. Perez-Hernandez J, Redon J, Cortes R. 2017. Extracellular Vesicles as Therapeutic Agents in Systemic Lupus
653 Erythematosus. Int J Mol Sci 18.
654 46. Cai Q, Qiao L, Wang M, He B, Lin FM, Palmquist J, Huang SD, Jin H. 2018. Plants send small RNAs in
655 extracellular vesicles to fungal pathogen to silence virulence genes. Science 360:1126-1129.
656 47. He B, Cai Q, Qiao L, Huang C-Y, Wang S, Miao W, Ha T, Wang Y, Jin H. 2021. RNA-binding proteins
657 contribute to small RNA loading in plant extracellular vesicles. Nature Plants doi:10.1038/s41477-021-
658 00863-8.
659 48. Klebanoff SJ, Kettle AJ, Rosen H, Winterbourn CC, Nauseef WM. 2013. Myeloperoxidase: a front-line
660 defender against phagocytosed microorganisms. J Leukoc Biol 93:185-98.
661 49. Hess C, Sadallah S, Hefti A, Landmann R, Schifferli JA. 1999. Ectosomes released by human neutrophils are
662 specialized functional units. J Immunol 163:4564-73.
663 50. Desai JV, Lionakis MS. 2018. The role of neutrophils in host defense against invasive fungal infections. Curr
664 Clin Microbiol Rep 5:181-189.
665 51. Edgar JR. 2016. Q&A: What are exosomes, exactly? BMC Biol 14:46.

666

667

668 **FIGURES AND FIGURE LEGENDS**

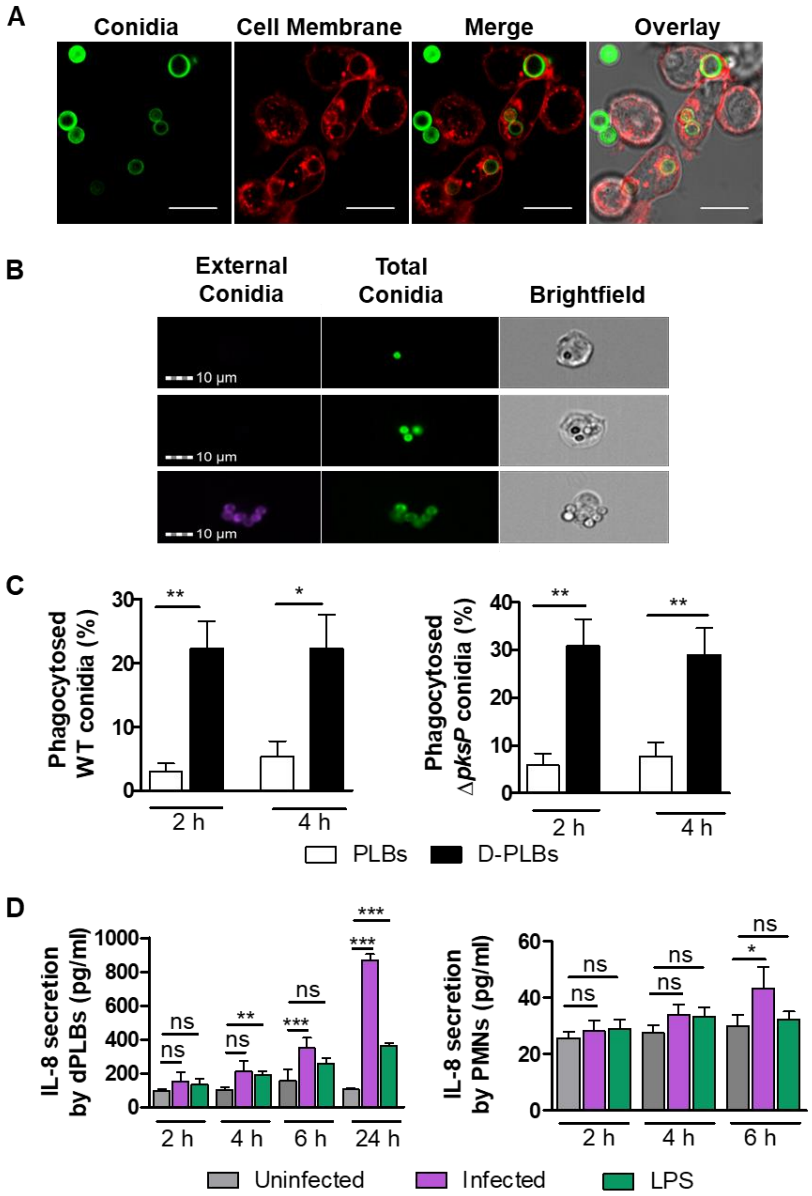

669

670 **FIG 1. Phagocytosis of *A. fumigatus* conidia by PLB-985 cells.**

671 **(A)**. Confocal microscopy images of wild-type conidia (FITC-stained; green) phagocytosed by dPLB cells after 4
672 hours co-incubation. Membranes were stained with Cell Mask (red). Images are representative of three
673 independent biological experiments. Scale bars are 10 µm. **(B)** Representative images of wild-type FITC-stained
674 conidia phagocytosed by dPLB cells after 4 hours co-infection obtained by imaging flow cytometry (top two rows).
675 External conidia are visualized by counter staining with CFW (purple), as seen in the bottom row. Images are
676 representative of three independent experiments. **(C)** Quantification of PLB-985 cell phagocytosis using the IDEAs
677 software on 5,000 cells per condition with either wild-type or Δ*pksP* conidia from four independent experiments

678 **(D)** ELISA detection of IL-8 cytokine released from infected dPLBs and primary human PMNs at different time
679 points. Lipopolysaccharide (LPS) was included for comparison of a bacterial stimulus. Data are presented as mean
680 ±SD, from six biological replicates; * = $p < 0.05$.
681

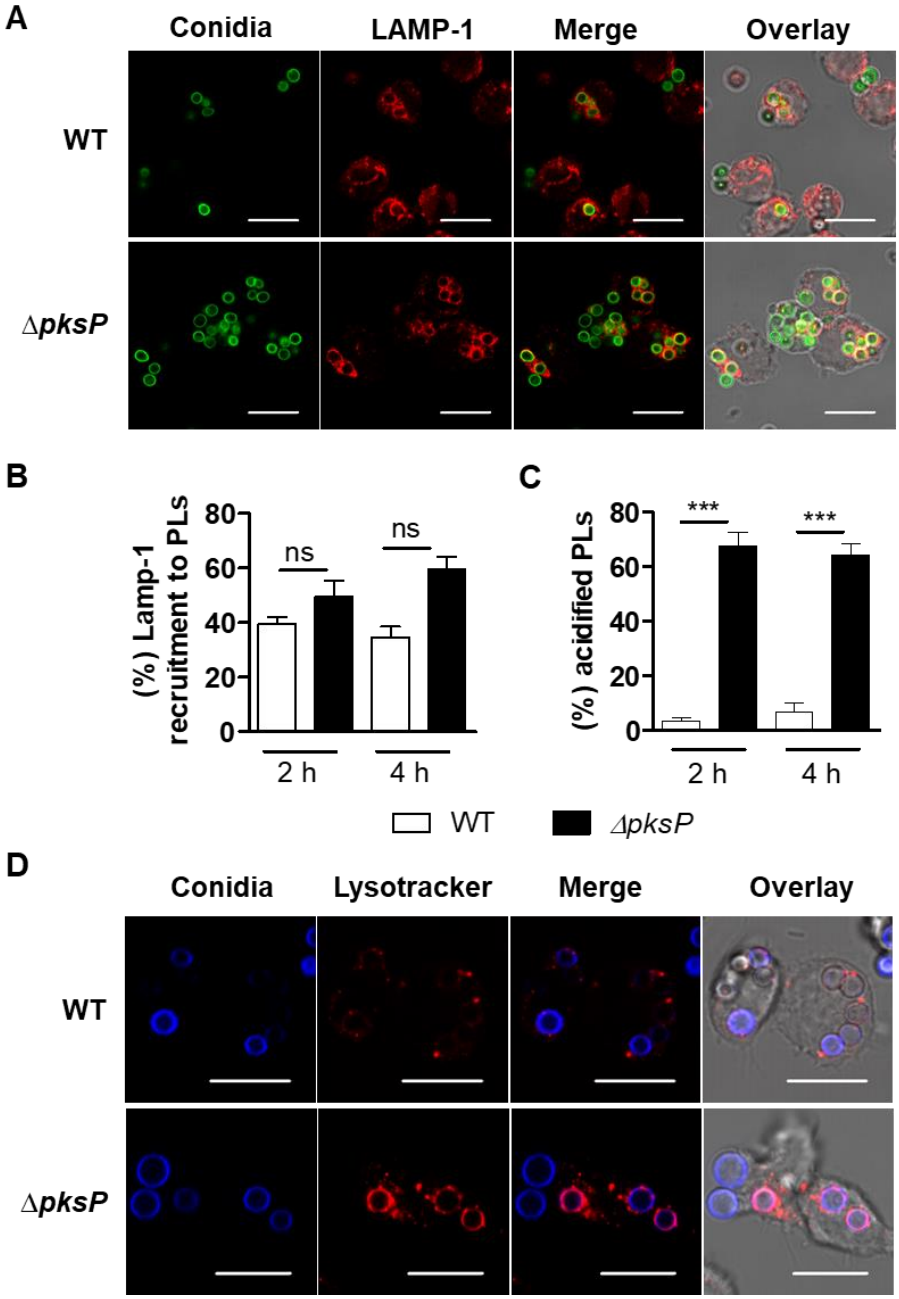

682
683 **FIG 2. Processing of *A. fumigatus* conidia inside phagolysosomes.**
684 **(A)** dPLB cells were stained with LAMP-1 (red) after infection with wild-type or Δ*pksP* conidia (FITC labeled; green)
685 for 4 h. Images are representative of three biological replicates. **(B)** Quantification of LAMP-1 co-localization with
686 CFW-labelled conidia in phagolysosomes and **(C)** Percentage of acidified conidia in dPLB cells after 2- and 4-hours

687 post-infection with wild-type and Δ*pksP* conidia. Data are presented as mean ±SD; *** = p < 0.001. **(D)**
688 Colocalization of conidia (CFW; blue) in acidified compartments labeled with Lysotracker (red). Images are
689 representative of three biological replicates. Scale bars are 10 µm.
690
691

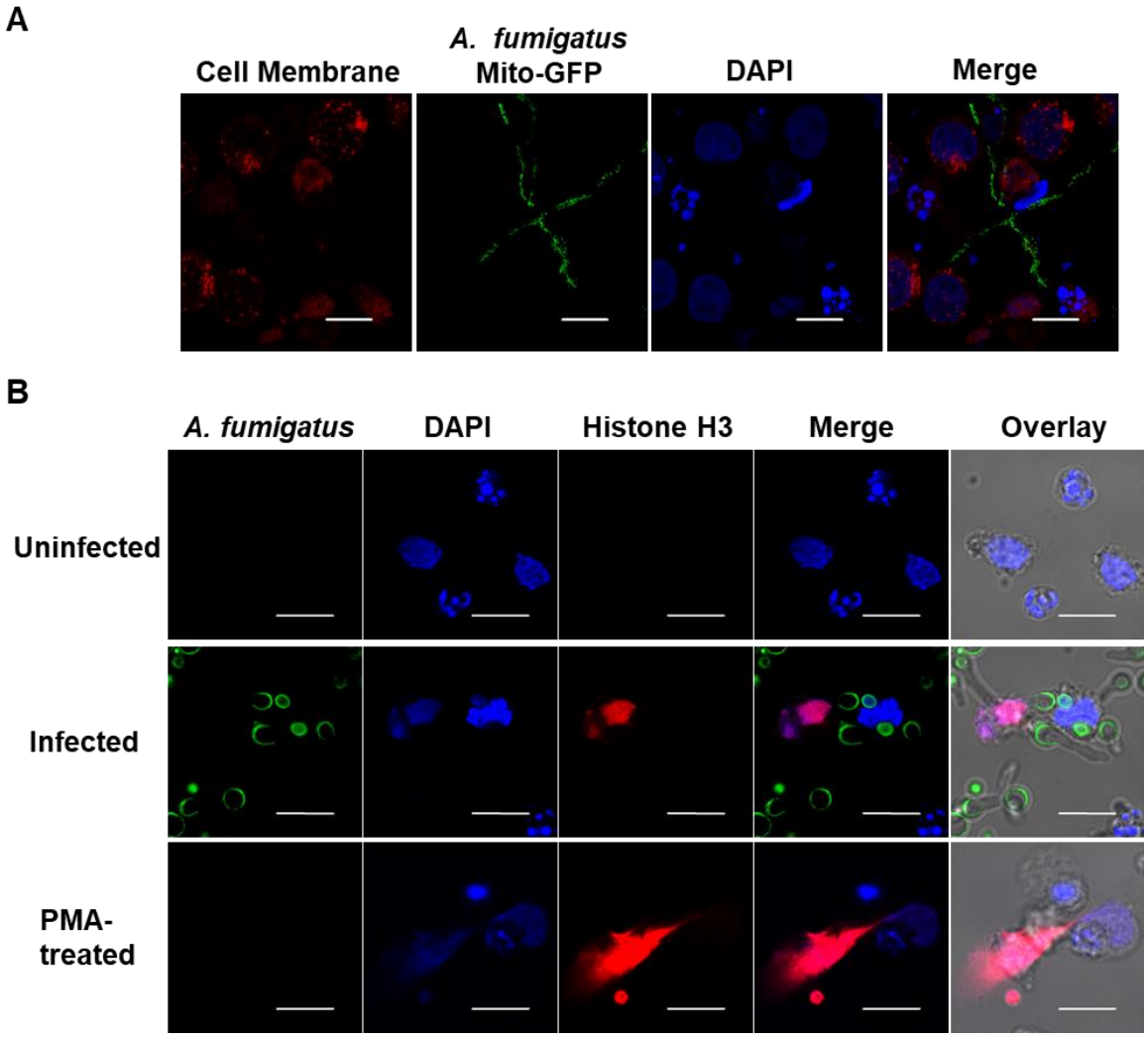

692
693 **FIG 3. Production of NETs in response to *A. fumigatus* infection**.
694 **(A)** Confocal scanning laser microscopy of nucleic acid stained with DAPI (blue) released from dPLB cells stained
695 with Cell Mask (red) after challenge with fungal hyphae containing a mitochondrial GFP reporter (*A. fumigatus*
696 strain AfS35 / pJW103 expressing a mitochondrial GFP reporter; green). Phorbol myristate acetate (PMA) was
697 used as a positive control. Data representative of three biological replicates. **(B)** Confocal micrographs of NET
698 markers, Histone H3 (red) and nucleic acid stained with DAPI (blue), produced by dPLB cells after contact with *A.*

699 *fumigatus* hyphae (FITC-labeled; green). Images are representative of three biological replicates. Scale bars are 10

700 µm.

701

702

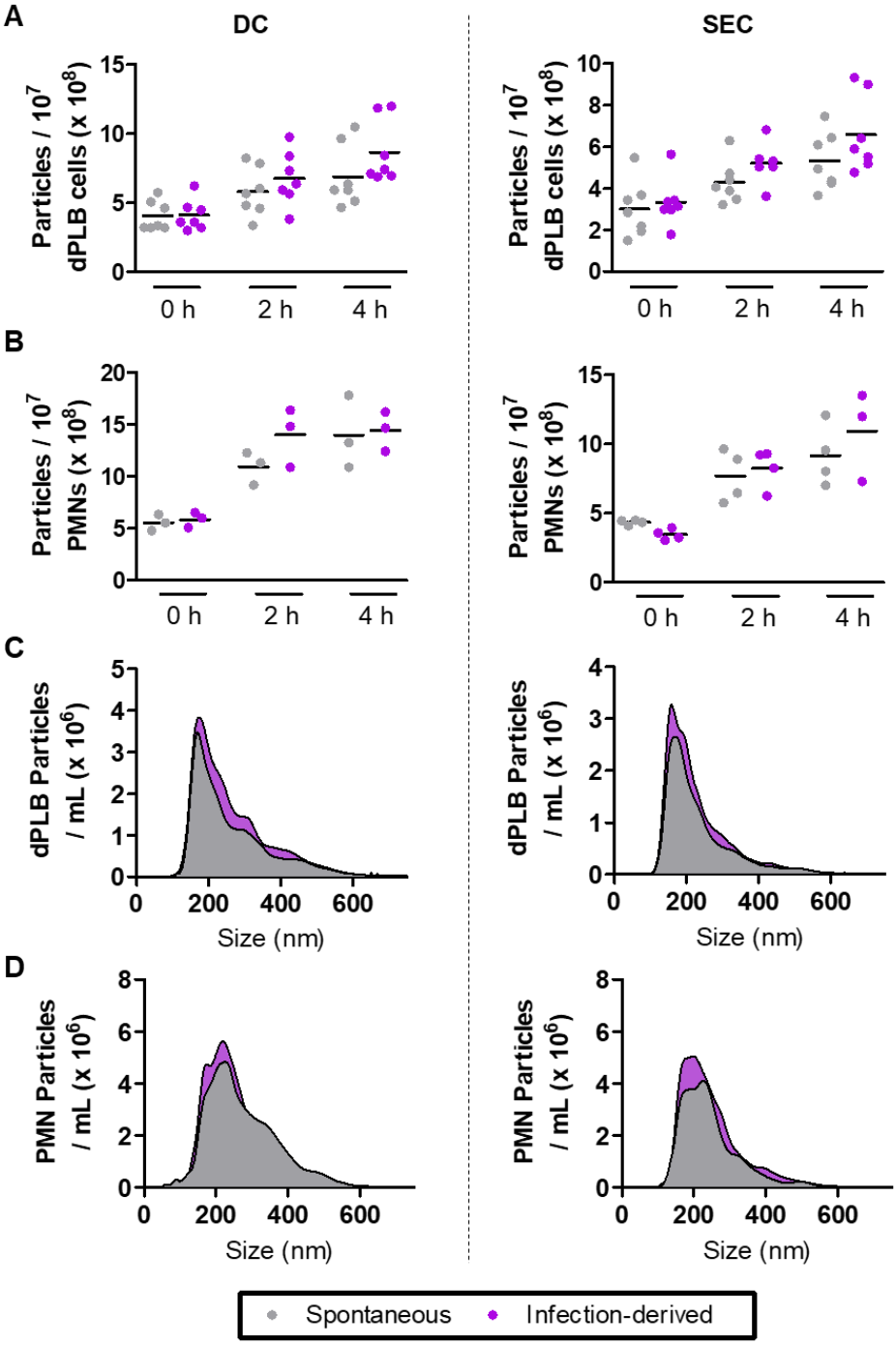

703

704 **FIG 4. dPLB cells produce extracellular vesicles comparable in size to primary human PMNs.**

705 Extracellular vesicles released spontaneously or produced in response to infection with opsonized *A. fumigatus*
706 conidia were isolated using a differential centrifugation-based approach (DC) or a size-exclusion chromatography-
707 based approach (SEC) and quantified using nanoparticle tracking analysis. Extracellular vesicles were quantified
708 from **(A)** dPLB cells or **(B)** primary human PMNs at 0, 2, and 4 hours post infection and show the average of at
709 least six biological replicates and three biological replicates, respectively. Representative size histograms from five
710 biological replicates are shown for extracellular vesicles derived from **(C)** dPLB cells and **(D)** primary human PMNs.
711
712

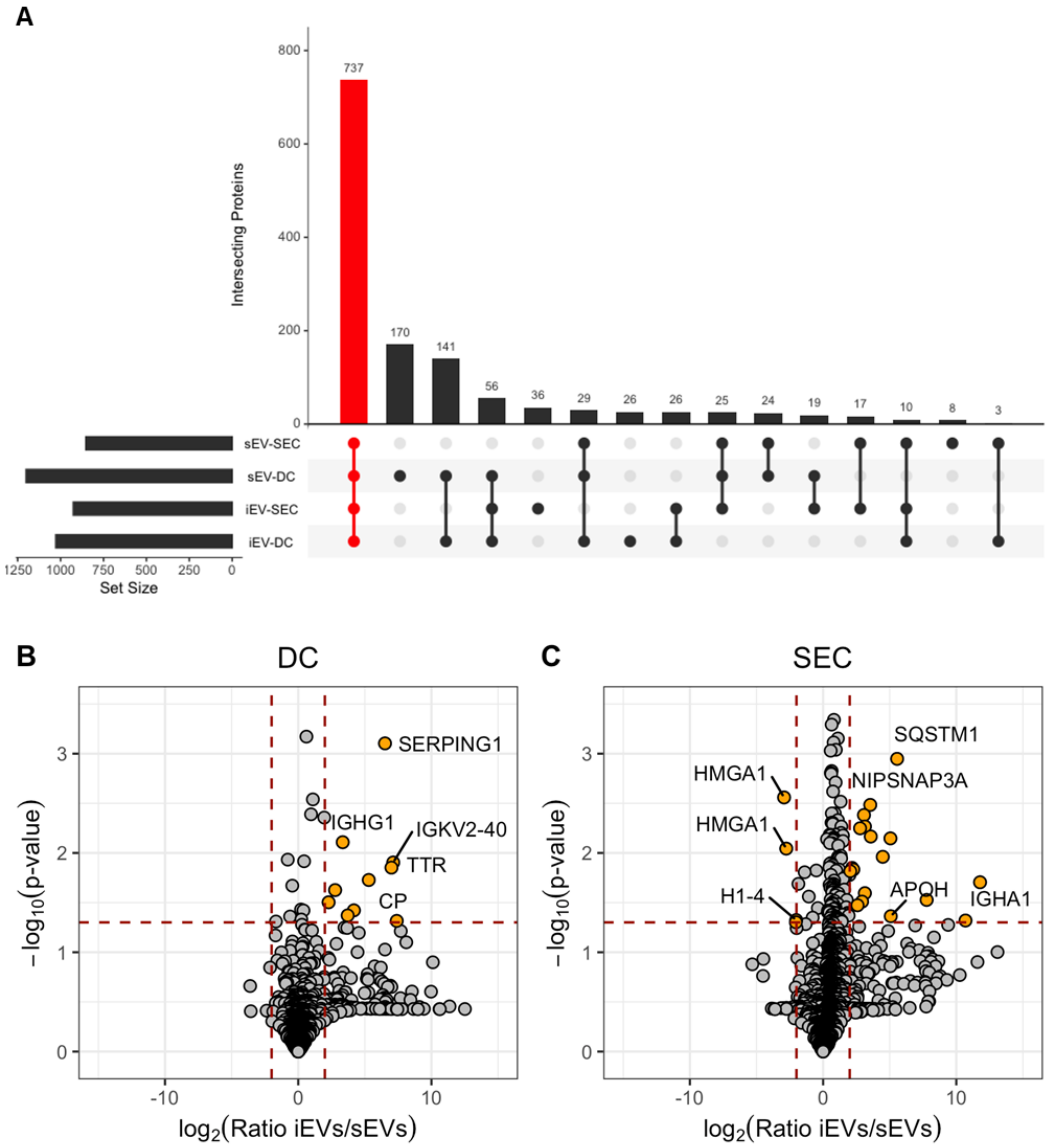

713
714 **FIG 5. SEC enriches for extracellular vesicle populations.**

715 LC-MS/MS proteomics analysis was performed on extracellular vesicles isolated from dPLB cells using a differential
716 centrifugation-based approach (DC) or a size-exclusion chromatography-based approach (SEC) in the presence or
717 absence of infection with opsonized *A. fumigatus* conidia. **(A)** Proteins identified in spontaneously released
718 extracellular vesicles (sEVs) and infection-derived extracellular vesicles (iEVs) from at least two replicates of a
719 given sample were intersected using UpSetR. The red bar indicates proteins that were found in all four samples.
720 Volcano plots show the $\log_2$ ratio of infection-derived extracellular vesicles (iEVs) versus spontaneously released
721 EVs (sEVs) for **(B)** DC-based isolation and **(C)** SEC-based isolation. Input data included values from all replicates
722 using the RMN data included in **Dataset S1**. Plots were created using ggplot2 in R. Proteomics data is from three
723 analytical replicates of three independent biological replicates. Orange circles represent proteins with greater
724 than 2-fold change and $p = < 0.05$. Selected proteins are named for clarity.
725
726

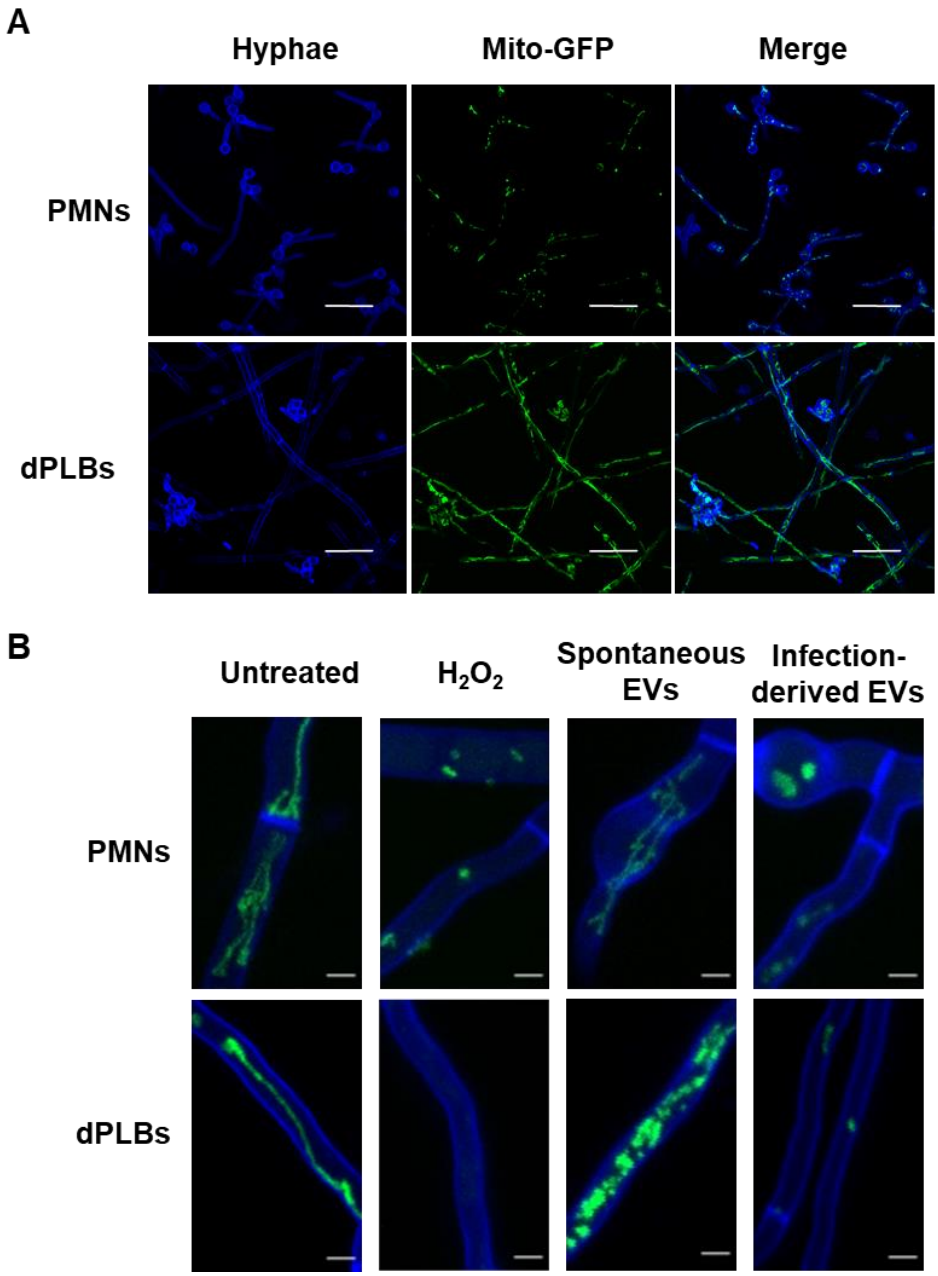

727

728 **FIG 6. Infection-derived extracellular vesicles from dPLBs are antifungal to *A. fumigatus* hyphae.**

729 **(A)** Conidia from *A. fumigatus* strain AfS35 containing plasmid pJW103 expressing a mitochondrial GFP reporter
730 (green) were opsonized and co-incubated with freshly harvested human PMNs or dPLBs. After overnight
731 incubation (22 hours) samples were stained with CFW for 10 min and images were taken using a Zeiss LSM 780
732 confocal microscope. Scale bars are 20 µm. **(B)** The *A. fumigatus* strain AfS35 expressing a mitochondrial GFP
733 reporter (green) was first grown for 6 hours and then stained with calcofluor white (blue) and incubated overnight
734 with spontaneously released extracellular vesicles or infection-derived extracellular vesicles isolated from primary
735 human PMNs or dPLBs. As a control, untreated hyphae and hyphae treated with 3 mM H_2O_2 to induce cell death

736 are included. An intact mitochondrial network is shown by a filamentous network, whereas a disrupted network
737 is shown by fragmentation or the lack of green signal. Scale bars are 5 µm.
738
739 **TABLES**
740 **Table 1. RMN-fold change of selected proteins identified in extracellular vesicles (EVs) from dPLB cells.**
741 Abbreviations: DC, differential centrifugation-based approach; SEC, size-exclusion chromatography-based
742 approach.

Gene	**Accession**	**Infection-derived EVs (DC) / Spontaneous EVs (DC)**	**Infection-derived EVs (SEC) / Spontaneous EVs (SEC)**	**Infection-derived EVs (SEC) / Infection-derived EV (DCs)**	**Spontaneous EVs (SEC) / Spontaneous EVs (DC)**
EV Markers					
CD63	F8VWK8	1.274	1.424	1.478	1.323
TSG101	F5H442	1.215	1.630	1.554	1.158
CD81	E9PRJ8	1.150	1.413	2.055	1.673
Non-EV Markers					
CANX (Calnexin)	P27824	-1.031	-1.082	-1.468	-1.398
MPO (Myeloperoxidase)	P05164	-1.024	1.026	2.063	1.963
CTSG (Cathepsin G)	P08311	1.045	1.042	1.117	1.120
AZU1 (Azurocidin)	P20160	-1.141	1.029	1.521	1.295

743
744
745
746
747
748
749
750

751
752
753 **SUPPLEMENTAL FIGURES**
754

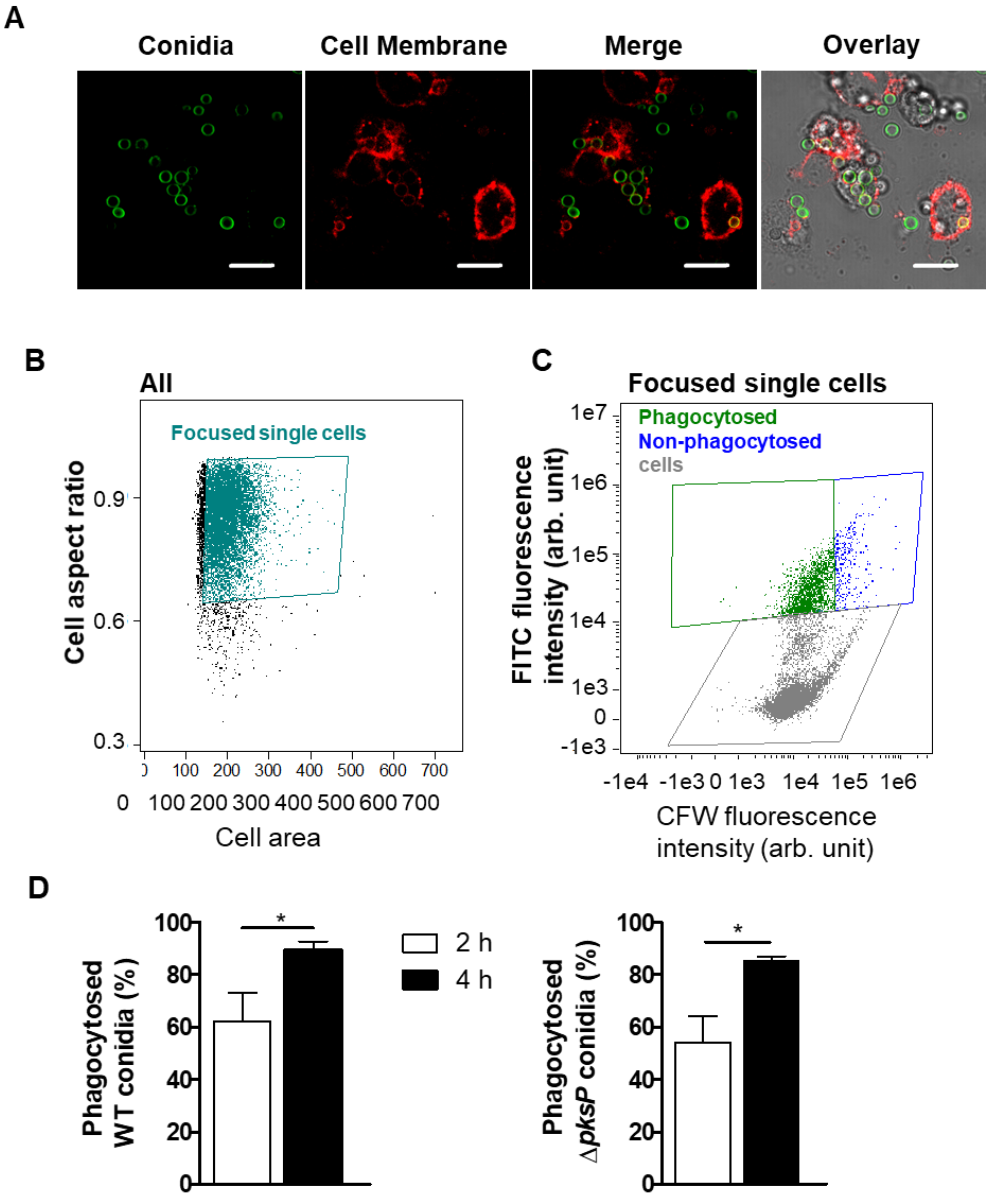

755
756 **FIG S1. Primary human neutrophils phagocytose wild-type conidia.**
757 **(A)** Confocal microscopy images of wild-type conidia (CFW-stained; false-colored green) phagocytosed by primary
758 human PMNs after 2 hours co-incubation. Membranes were stained with Cell Mask (red) to indicate cell
759 membranes. Images are representative of at least two independent biological experiments. Scale bars are 10 μm.
760 **(B and C)** indicate the gating strategy for determining phagocytosis rates of dPLB cells and PMNs using imaging
761 flow cytometry. **(B)** Single cell populations were selected based on their area and aspect ratio in the bright field
762 channel. **(C)** Phagocytosed conidia were gated based on their higher FITC fluorescence intensity and low CFW
763 fluorescence intensity. Cells without conidia had low FITC fluorescence intensity. The data subject to analysis

764 included only cells in focus and were pre-gated during data acquisition based on their high root mean square
765 gradient in the bright field channel. **(D)** Quantification of phagocytosis by primary human PMNs using the IDEAs
766 software on 5,000 cells per condition with either wild-type or Δ*pksP* conidia from four independent experiments.
767

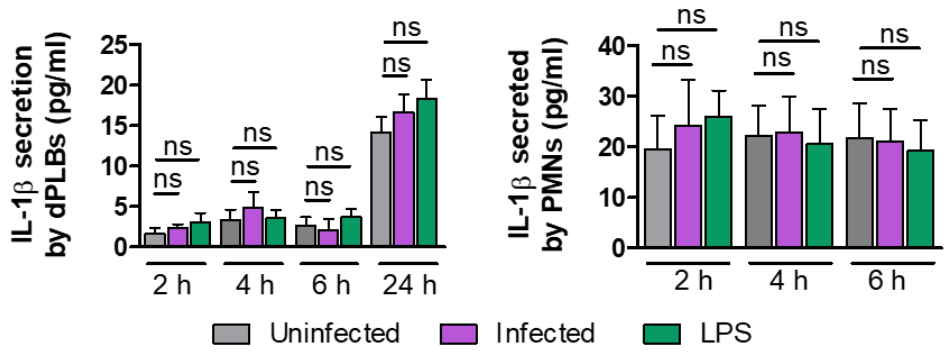

768
769 **FIG S2. Cytokine production by dPLB cells and PMNs.**
770 ELISA detection of the IL-1β cytokine released from infected dPLBs or primary human PMNs at different time
771 points. Lipopolysaccharide (LPS) was included as a comparison to a bacterial stimulus. Data are presented as mean
772 ±SD, from six biological replicates; * = $p < 0.05$.
773
774

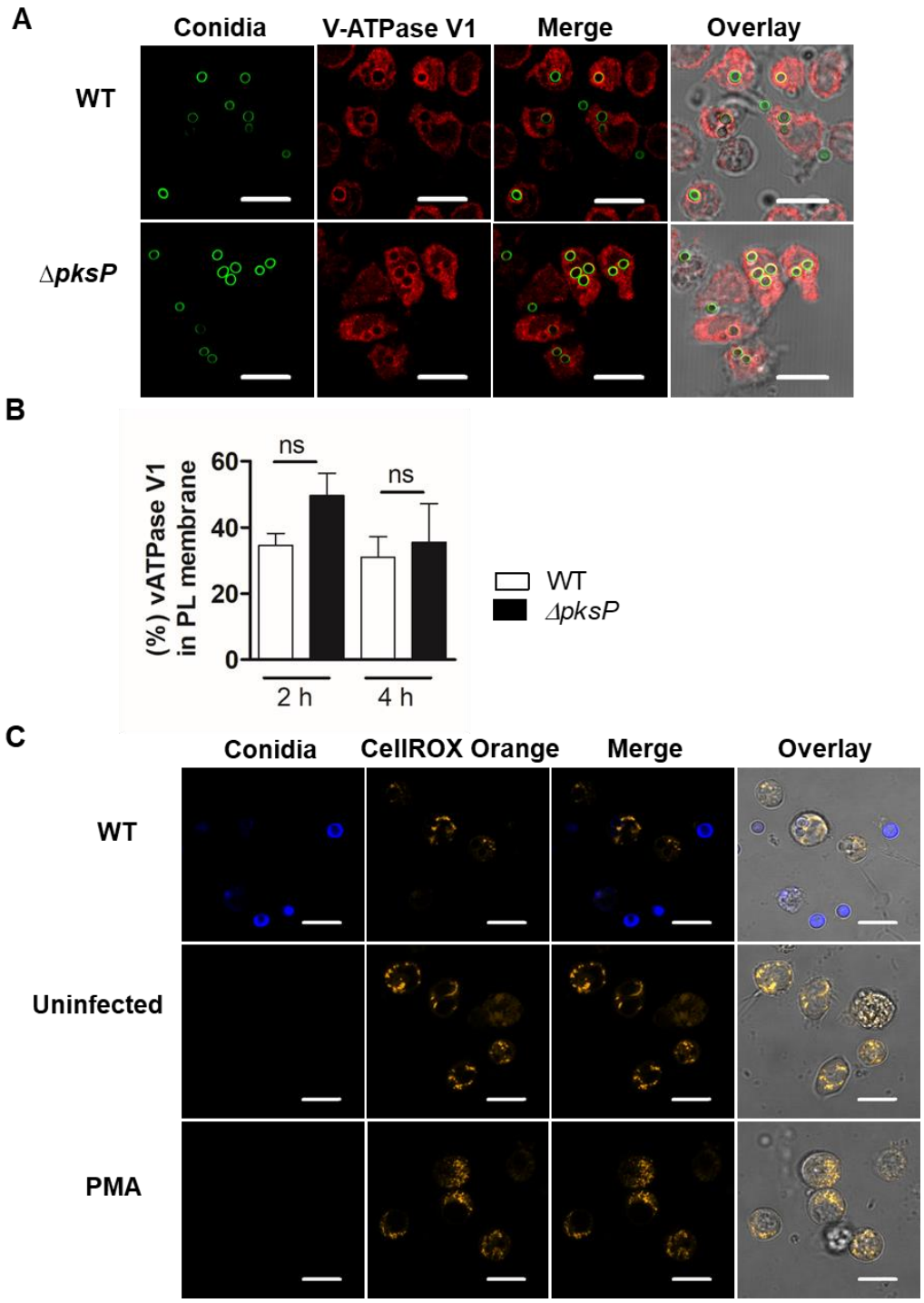

FIG S3. V-ATPase V1 localization to phagolysosomal membranes and ROS production by dPLB cells. **(A)** Immunofluorescence staining for V-ATPase V1 (red) in dPLB cells after infection with wild-type or Δ*pksP* conidia (FITC labeled; green) for 4 hours. Images are representative of three biological replicates. Scale bars are 10 µm. **(B)** Quantification of V-ATPase V1 positive phagolysosomes after 4 hours of infection with wild-type or Δ*pksP* conidia. Graphs are from three biological replicates. **(C)** Confocal microscopy images of dPLB cells infected with

781 wild-type conidia (CFW-stained; blue), left uninfected, or treated with PMA as a positive control and stained for
782 detection of reactive oxygen species using CellROX Orange stain.
783

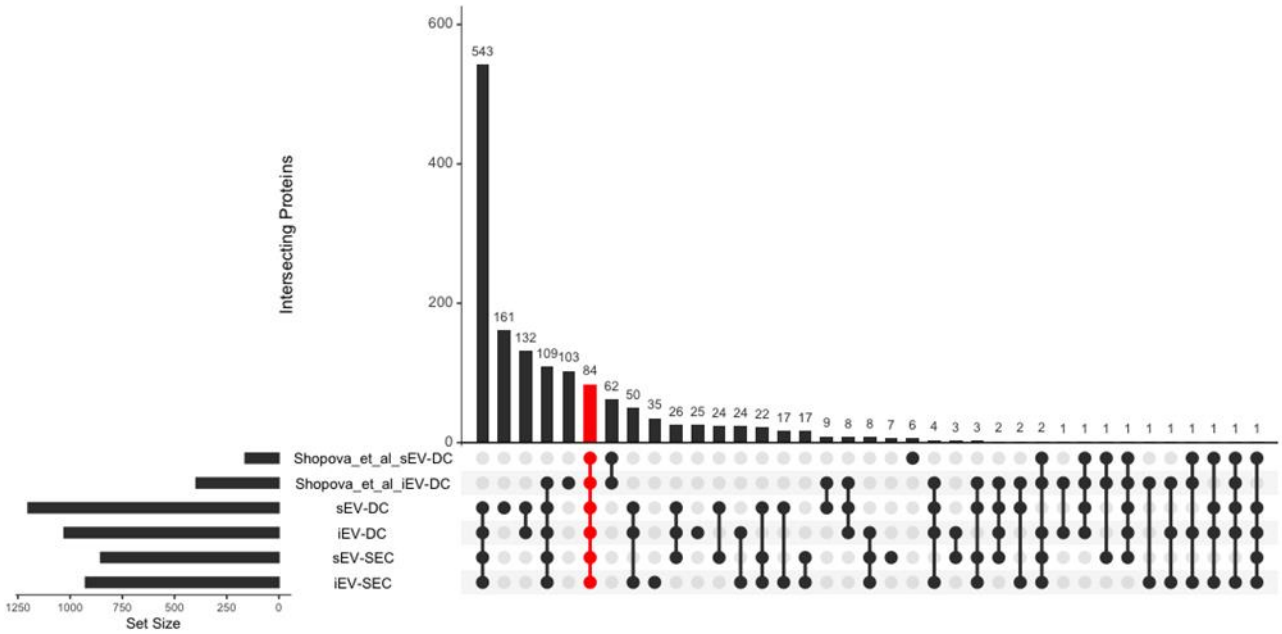

784
785 **FIG S4. Intersection of proteomics data with previously reported neutrophil-derived EV proteomes.**
786 LC-MS/MS proteomics analysis was performed on extracellular vesicles isolated from dPLB cells using a
787 centrifugation-based approach (DC) or a size-exclusion chromatography-based approach (SEC) in the presence or
788 absence of infection with opsonized *A. fumigatus* conidia and compared to data from (10). Proteins that were
789 identified in this study were compared to proteins identified by a similar approach using label-free quantification
790 from Shopova et al. (10). Proteins had to be found in at least two replicate of a given sample to be included in the
791 UpSetR analysis. The red bar indicates proteins that were found in all six samples.
792
793

794

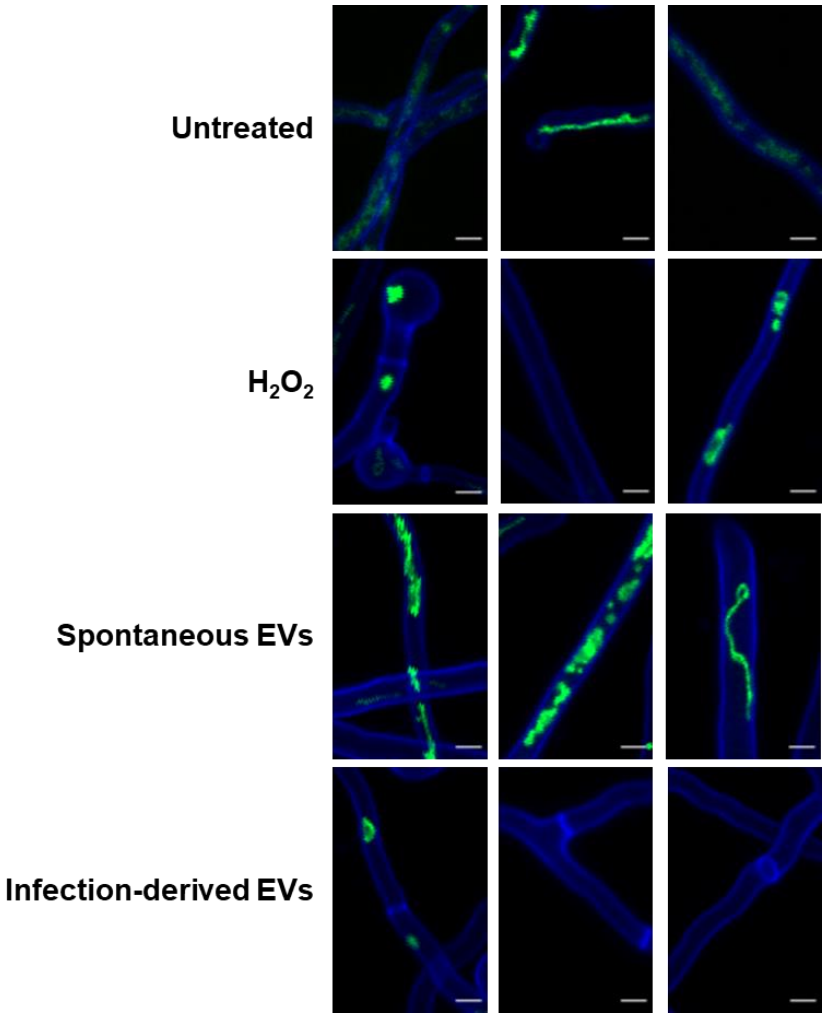

795

796 **FIG S5. Representative images of dPLB-derived extracellular vesicles effects on *A. fumigatus* hyphae.**
797 *A. fumigatus* strain AfS35 contains plasmid pJW103, which expresses a mitochondrial GFP reporter (green). The
798 strain was grown for 6 hours and then stained with calcofluor white (blue) and incubated overnight with
799 spontaneously released extracellular vesicles or infection-derived extracellular vesicles from dPLBs. Additional
800 representative images are included to show extent of variability that occurs in regard to extracellular vesicle killing
801 experiments shown in **Fig. 6**. As a control, untreated hyphae and hyphae treated with 3 mM H_2O_2 to induce cell
802 death are included. An intact mitochondrial network is shown by a filamentous network, whereas a disrupted
803 network is shown by fragmentation or the lack of green signal. Scale bars are 5 µm.

804

805 **SUPPLEMENTAL TABLES**

806

807 **Table S1. Proteins identified only in infection-derived extracellular vesicles (≥2 replicates) by both isolation**
808 **methods.** Abbreviations: PSMs, peptide spectrum matches; AAs, amino acids; Cov%, percent coverage of
809 mapped peptides.

810

Gene	Accession	Description	(PSMs/AAs)*(Cov%/100)
IGKC	P01834	Immunoglobulin kappa constant	3.45421
APOA1	P02647	Apolipoprotein A-I	1.73397
IGHM	P01871	Immunoglobulin heavy constant mu	1.26349
IGLC2	P0DOY2	Immunoglobulin lambda constant 2	0.82453
IGHG1	P01857	Immunoglobulin heavy constant gamma 1	0.51688
HBB	P68871	Hemoglobin subunit beta	0.43599
IGHG2	A0A286YEY4	Immunoglobulin heavy constant gamma 2 (Fragment)	0.27205
APOB	P04114	Apolipoprotein B-100	0.26471
IGHA1	P01876	Immunoglobulin heavy constant alpha 1	0.16677
C1QB	P02746	Complement C1q subcomponent subunit B	0.16126
NPTN	Q9Y639	Neuroplastin	0.12879
APCS	P02743	Serum amyloid P-component	0.12233
C1QC	P02747	Complement C1q subcomponent subunit C	0.07286
APOH	P02749	Beta-2-glycoprotein 1	0.06858
APOD	P05090	Apolipoprotein D	0.06349
EMB	D6RDX7	Embigin	0.04667
CFH	P08603	Complement factor H	0.02729
IGKV2-40	A0A087WW87	Immunoglobulin kappa variable 2-40	0.02545
DNAJA1	P31689	DnaJ homolog subfamily A member 1	0.01884
HPX	P02790	Hemopexin	0.01541
C4B	F5GXS0	C4a anaphylatoxin	0.00783
FN1	P02751	Fibronectin	0.00560
C3	P01024	Complement C3	0.00394
C8A	P07357	Complement component C8 alpha chain	0.00394
AHSG	P02765	Alpha-2-HS-glycoprotein	0.00229
C1R	B4DPQ0	Complement subcomponent C1r	0.00118

811

812

813 **SUPPLEMENTAL DATASETS**

814

815 **Dataset S1. Proteomics data of extracellular vesicles produced in response to *A. fumigatus* infection by dPLB**
816 **cells.**

817